ABSTRACT

COULOMB DISPLACEMENT ENERGIES OF $1f_{7/2}$ SHELL MIRROR NUCLEI

by Dennis Warren Mueller

The Q-values of the $^{46}Ti(^{3}He,^{6}He)^{43}Ti$, $^{50}Cr(^{3}He,^{6}He)^{47}Cr$, $^{54}Fe(^{3}He,^{6}He)^{51}Fe$ and $^{58}Ni(^{3}He,^{6}He)^{55}Ni$ reactions have been measured and the mass excesses of of the T_z=-1/2 residual nuclei deduced. The exitation energies of several levels below 7 MeV in the final nuclei were measured. Angular distributions of the $J^{\pi}= 7/2^{-}$, $3/2^{+}$ and $1/2^{+}$ levels were taken and compared to those from the $^{42}Ca(^{3}He,^{6}He)^{39}Ca$ reaction.

The measurements were made using the 70 MeV. ^{3}He beam from the Michigan State University Cyclotron. The ^{6}He particles were detected in the focal plane of an Enge split-pole magnetic spectrograph by two resistive-wire gas-proportional counters and a plastic scintillator.

The Coulomb displacement energies of the $7/2^{-}$, $3/2^{+}$ and $1/2^{+}$ levels of the A=4n+3, T=1/2 mirror nuclei in the $1f_{7/2}$ shell were extracted and compared to calculations. The new mass values were employed in the Garvey-Kelson Symmetric Mass relation to predict the mass of 32 proton-rich nuclei with T>1/2 from Vanadium through Nickel.

COULOMB DISPLACEMENT ENERGIES OF $1f_{7/2}$ SHELL MIRROR NUCLEI

by

DENNIS WARREN MUELLER

A THESIS

Submitted to
Michigan State University
in partial fulfillment of the requirements
for the degree of

DOCTOR OF PHILOSOPHY

Department of Physics

1976

ACKNOWLEDGMENTS

I would like to express my sincere appreciation to the faculty and staff of the Cyclotron laboratory for their support during my graduate study at Michigan State University.

In particular, I wish to thank Professor Walter Benenson and Dr. Herman Nann for their help in acquiring some of the data for this thesis as well as Steve Motzny for his help in preparing some of the figures. I am indebted to Dr. Roger Markham for valuable discussions on detector design and to Norbal Mercer and his staff for their help in fabricating the detectors.

I am especially grateful to Professor Edwin Kashy for suggesting this topic and for his guidance during the work for this thesis.

Finally, I wish to thank my wife, Linda, for typing the manuscript and for her patience and support throughout my graduate study.

TABLE OF CONTENTS

LIST OF TABLES

LIST OF FIGURES

1. INTRODUCTION

Mirror nuclei are those nuclei which can be made from each other by interchanging all protons and neutrons. Under the assumption that the nuclear part of the nucleon-nucleon force does not depend on whether neutrons or protons are involved, the binding energies of two mirror nuclei differ only by the Coulomb interaction of the protons. This difference in the binding energy is called the Coulomb displacement energy (ΔE_c). The Coulomb displacement energies of mirror nuclei were first measured by determining E_{max} of the β^+ particles emitted in the decay of the proton rich member of mirror pairs. Then ΔE_c is just $E_{max}+m_oc^2 + (M_n-M_p)c^2$ where m_o is the electron mass and (M_n-M_p) is the neutron-proton mass difference.[Ev55] Currently, however, accurate measurement of the masses of nuclei in magnetic spectrographs can be used to determine ΔE_c to the accuracy of a few keV. The experimental value of the Coulomb displacement energy between two isobaric nuclei differing by one unit of charge is given by

$$\Delta E_c = M(Z_>) - M(Z_<) + (M_n - M_p)$$

where $M(Z_>)$ [$M(Z_<)$] denotes the mass of the nucleus with the greater [fewer] number of protons.

Historically, Coulomb displacement energies have been employed to provide information on the nuclear charge radius. Evans ^{Ev55}, for example, discusses nuclear radii extracted from several different types of data including Coulomb displacement energies. He assumes a homogenously charged spherical nucleus and finds $\Delta E_c = 6/5 \frac{Z_< e^2}{R}$ for the Coulomb energy difference between two mirror nuclei differing by one unit of charge. Here $Z_< e$ denotes the charge of the neutron-rich member of the pair. Evans then used the existing data on mirror nuclei to find $R \tilde{=} 1.45 A^{1/3}$fm. And, he also notes that since the Beta transformed nucleon should be near the nuclear surface, the radius may be as small as $R \tilde{=} 1.2 A^{1/3}$fm. Bohr and Mottelson^{Bo69} use the semi-empirical mass formula of Weizsacker^{We35}

$$B.E. = b_{vol} A - b_{surf} A^{2/3} - 1/2\, b_{sym} \frac{(N-Z)^2}{A} - 3/5 \frac{Z^2 e^2}{R}$$

for the binding energy of the nucleus and find $R = 1.24 A^{1/3}$fm in agreement with Evans. With the discovery of Isobaric analogue states in nuclei, it became possible to extract Coulomb displacement energies between two nucleii having the same mass number, Isotopic spin and nuclear structure. This allows the extraction of nuclear charge radii for all nuclear states, except T =0, whose Isobaric analogues are known. However, current results of electron scattering and muonic X-rays yield more precise values for the nuclear charge radius of the ground states of stable nuclei.

Nolen and Schiffer[No69] report that the charge radii extracted from Coulomb displacement energies are smaller by 2 to 7 percent than those measured by electron scattering or muonic X-rays, and that this discrepancy persists even when a better independent particle model such as harmonic oscillator or Woods-Saxon wells are used.

Nolen and Schiffer posed the problem differently by saying in effect that Coulomb displacement energies cannot be used to extract accurate charge radii, but rather, the radii accurately known from electron scattering or muonic X-rays should be employed as a starting point for calculating the Coulomb energy shifts between nuclei. They found, for example, that if the known charge radius of a closed ^{40}Ca core and a Woods-Saxon or harmonic oscillator wave-function for the orbiting nucleon in ^{41}Ca were used, that the calculated Coulomb displacement energy for ^{41}Ca -^{41}Sc is too small. They found ΔE_c calculated in this manner to be 8-10% smaller than the experimental values for a wide range of nuclei. This discrepancy persists when both the exchange and electromagnetic spin-orbit terms are included. They suggested that a possible solution to this dilemma was that the radius of the particles outside the closed core was 6 to 20% smaller than expected. After investigating different shapes of the core charge distribution, they concluded that the calculated ΔE_c depended most strongly on the root-mean-square radius but very little on the specific shape of the distribution. After discussing several other possible corrections to ΔE_c, Nolen and Schiffer concluded that either the rms radius of the last neutron is much smaller than expected or that some large correction term had been neglected. This discrepancy, called the Nolen-Schiffer anomaly, has been the subject of several theoretical papers in recent years.[Au72, Sh75b, Lo76, No71, No74, Sh73, Sh72, Ok71, Sa76] These papers have considered various possible solutions to this anomaly including vacuum polarization, higher order magnetic terms, the finite size of the proton, the proton-neutron mass difference and Isospin mixing in the core. Also considered is the possibility that the specifically nuclear part of the p-p interaction differs from the n-n interaction, called charge-symmetry breaking. Shlomo and collaborators[Sh75b, Lo76] and Sato[Sa76] have made detailed calculations of the Coulomb, magnetic, vacuum polarization, p-n mass difference and Isospin mixing parts of ΔE_c and attempted to assign the remainder to a charge symmetry breaking potential. Although improvements have been made in the theoretical calculations of Coulomb displacement energies, the predicted values continue to underestimate the effect.

In this work, a method for measuring nuclear reaction Q-values of multi-nucleon transfer reactions in a magnetic spectrograph is discussed. The method is essentially an extension of the techniques described by Kashy et al.[Ka73] A beam from the Michigan State University Cyclotron is used to induce charged particle reactions, such as ^{58}Ni(^{3}He,^{6}He)^{55}Ni. The products from a reaction whose Q-value is to be measured are magnetically analyzed in an Enge split-pole spectrograph and compared to the magnetic rigidities of similar reaction products from a known reaction. The principal differences between the current and previous methods are that more rigorous particle identification has been made possible and that detectors which can achieve better spatial resolution have been developed. Previously particle identification was achieved primarily by the specific ionization of the detected ions in a single gas-proportional counter and by the time of flight of the particles through the spectrograph. In the current work, a second proportional counter was employed to give redundant ΔE information. Also, use of thin (.23 mm) plastic scintillator aided in reducing the background and better design of the light pipes made the total light output from the scintillator more useful. Finally, use of event recording in the current work has proved to be superior to taking live data. This superiority results from being able to replay the data while making successive refinements in the requirements for particle identification. Better resolution was achieved by employing thinner resistive-wire gas-proportional counters than previously, as well as by using thinner targets. Continued refinements in the present methods should help to push back the frontier of unknown nuclei.

The results of employing this method to remeasure the Q-values of the $^{46}Ti(^{3}He,^{6}He)^{43}Ti$, $^{50}Cr(^{3}He,^{6}He)^{47}Cr$, $^{54}Fe(^{3}He,^{6}He)^{51}Fe$ and $^{58}Ni(^{3}He,^{6}He)^{55}Ni$ reactions are discussed. Also presented are the mass-excesses deduced for the residual nuclei, the excitation energies of several levels in these nuclei and angular distributions for a few of the more strongly populated levels. The high-intensity 70 MeV ^{3}He beam from the MSU Cyclotron made the latter possible using runs of a few hours at each detection angle.

The current experimental results are of interest since they allow accurate determination of Coulomb displacement energies for the ground and a few excited states of T=1/2 mirror nuclei throughout a nuclear subshell. While the displacement energies between isobaric analogue states in heavier nuclei are known, the current results include the heaviest known mirror nuclei. The displacement energy of a mirror pair is expected to depend only on the Coulomb interaction and possibly a charge-symmetry-breaking nuclear force, i.e., a difference in the nuclear part of the p-p and n-n interactions. The displacement energy of a non-mirror isobaric analogue pair may depend, in addition, upon a charge dependent nuclear force, i.e., a difference in the T=1, p-n and n-n interactions. Hence, it may be possible to extract the p-n and n-n difference by comparing the displacement energies of higher T isobaric analogue pairs to those of the T=1/2 mirror pairs.

The results for the Coulomb displacement energies are compared to a shell-model prediction and to a model for the Coulomb energies of excited particle-hole states.[Sh75] Finally, the current values of the masses are used in the Garvey-Kelson symmetric mass relation to predict the masses of proton-rich nuclei in the $1f_{7/2}$ shell.

2. EXPERIMENTAL PROCEDURE

INTRODUCTION

The remeasurement of the masses of and the determination of the levels of ^{43}Ti, ^{47}Cr, ^{51}Fe and ^{55}Ni were made by comparing the ^{6}He particles from the (^{3}He,^{6}He) reaction on ^{46}Ti, ^{50}Cr, ^{54}Fe and ^{58}Ni to the ^{6}He particles from the (^{3}He,^{6}He) reaction on ^{27}Al and ^{25}Mg in a magnetic spectrograph. The low yield from these reactions when using thin targets, 40 to 324 μg/cm^{2}, necessitated high beam intensities, 1 to 3 μA, long runs, 5 to 30 millicoulombs of integrated beam current and a powerful particle identification system. The Michigan State University Cyclotron provided the stable high-intensity beam of 70 MeV ^{3}He particles necessary for the measurements. The particle-identification system consisted of two resistive-wire-proportional counters backed by a plastic scintillator. The two proportional counters provided redundant information of energy loss in the gas, while the signal from the plastic scintillator was employed to give both time of flight in the spectrograph and light-output information.

Angular distributions of the (^{3}He,^{6}He) on ^{46}Ti, ^{50}Cr, ^{54}Fe and ^{58}Ni were taken as far back as 27 deg. in the laboratory despite the low cross sections, 0.1 to 1.1 μb/sr, of even the most prominent peaks in the spectra of the final nuclei. The low cross sections necessitated the use of thick targets, about 1 mg/cm^2, in obtaining the angular distributions.

2.1 PARTICLE IDENTIFICATION

The reaction particles were identified by means of their specific ionization in a double-wire gas proportional counter, their time of flight through the spectrograph and their total light output in a plastic scintillator. Figure 2.1.1 illustrates the electronics for this system.

The specific ionization of a particle with a given energy can be found in Nuclear Data Tables No70 and Reference Wi66. In a spectrograph it is convenient to know the specific ionization as a function of magnetic rigidity of the particles. Figure 2.1.2 is a graph of the specific ionization of various ions in Propane versus magnetic rigidity. While several ion species can be identified by means of their specific ionization, some such as ^{7}Be and ^{7}Li or ^{6}He and ^{6}Li cannot be separated by this means. This ambiguity arises from the considerable overlap in the energy loss spectrum of particles with others having nearly the same specific ionization. Furthermore, particles with low specific ionization have a small probability of having a large energy loss in the gas due to the very long tail of the energy loss distribution.[Ko68] An anomalously large energy loss from a prolific light ion can present an ambiguity in identifying heavier ions from low cross section reactions. A second proportional counter is employed to provide redundant energy loss information. The probability of a light particle producing an anomalously large signal in both the first and second detectors is small. For instance, the calculated probability of an alpha particle yielding an energy loss signal equivalent to that of a ^{6}He particle is about $3\text{x}10^{-4}$ Ko68 for a single proportional counter, while for a double proportional counter this probability is about $1\text{x}10^{-7}$. Experiment indicates that the probability calculated assuming a Vavilov distribution for a single proportional counter is about an order of magnitude too small.

The time of flight of the reaction particles in the spectrograph is essential in particle identification. The speed of a charged particle through the spectrograph is directly proportional to its effective radius of curvature, ρ in cm., while the length of the flight path is: $L = (54.7 + 3.61\rho - .00294\rho^2)$ cm. Mi76 For 80 cm. $> \rho >$ 70 cm., which corresponds to a distance of 25 cm. along the focal plane, the time-of-flight in the spectrograph varies only by about 2%. Therefore, the time-of-flight of an ion species is about the same at all points along a detector in the focal plane. Figure 2.1.3 shows the time-of-flight spectra for several ion species. The time is measured by using the anode signal from the photomultiplier on the plastic scintillator as a start pulse and the r.f. signal from the cyclotron as the stop pulse in a time-to-amplitude converter (T.A.C.). Thus, in the time-of-flight spectrum, the fastest ion species yields the largest signal from the T.A.C. The time resolution is strongly affected by the angular spread accepted by the spectrograph entrance aperture. The data in Figure 2.1.3. taken with a $2^o x 2^o$ aperature, clearly shows that the slower ion species have a broader time-of-flight peak. The ratio of the widths of the proton to triton peaks is 5:12 instead of 1:3 which is predicted from the ratio of the velocities of the particles, under the assumption of no contribution from the beam or detection system. The small departure from a ratio of 1:3 implies a contribution of less than 1. ns. to the resolution from the beam and detection system. Since the time of flight of an ion through the spectrograph is inversly proportional to its charge to mass ratio, there is an ambiguity in the identification of particles having the same charge to mass ratio. This ambiguity is removed by the energy loss in the gas of the proportional counters as Figure 2.1.4 indicates. A 74. Mev. ^{3}He beam incident on a ^{13}C target produced the reaction products for the plot of time of flight versus energy loss shown in Figure 2.1.5. In this figure, particles having a low specific ionization were eliminated by means of a coincidence requirement that their energy-loss signal be at least as large as that of ^{6}Li ions having the same magnetic rigidity. It is clear from Figure 2.1.5 that the combination of time-of-flight and energy loss information is a powerful particle identification scheme.

There is one further piece of information available for particle discrimination and that is the total light output of the particle in the plastic scintillator. Because gamma rays and neutrons arrive at the detector at all times, a gamma ray or neutron could trigger the T.A.C. and produce a time-of-flight signal equal to that of the particle of interest. This time signal in coincidence with an anomalously large energy-loss signal from a lightly ionizing particle or with a large energy-loss signal due to pileup of light ions could cause misidentification of the event. However, a low level discriminator is used to analyze the anode signal before it can start the T.A.C. This low level discrimination helps to eliminate random time signals produced by gamma rays and neutrons since the light output from these particles is generally smaller than those for the particles of interest. Figure 2.1.6 shows a plot of light output versus magnetic rigidity for various particle types stopping in the scintillator.[Be75] The total light output is useful for redundant particle identification, as well as for discrimination against gamma rays and neutrons. The use of very thin (.23 mm.) scintillator aids in the reduction of the neutron and gamma-ray background. Furthermore, lightly ionizing particles pass through the thin scintillator producing only small light signals, thereby facillitating identification of the heavier particles. Resolution of the light output spectrum is limited by the light collection efficiency which varies with position in the detector. A plot of the light output versus position in a typical detector is shown in Figure 2.1.7. Use of a two-dimensional gate for light as a function of position can improve the usefulness of the light output information. Such gates are made possible by the use of the computer programs III EVE and EVEN.[Au76]

By employing the particle discrimination system described above, cross-sections as low as 7 nb/sr have been observed, and the use of exotic transfer reactions such as (^{3}He,^{8}Li), (^{3}He,^{8}B) and (^{3}He,^{9}C) has been made possible.

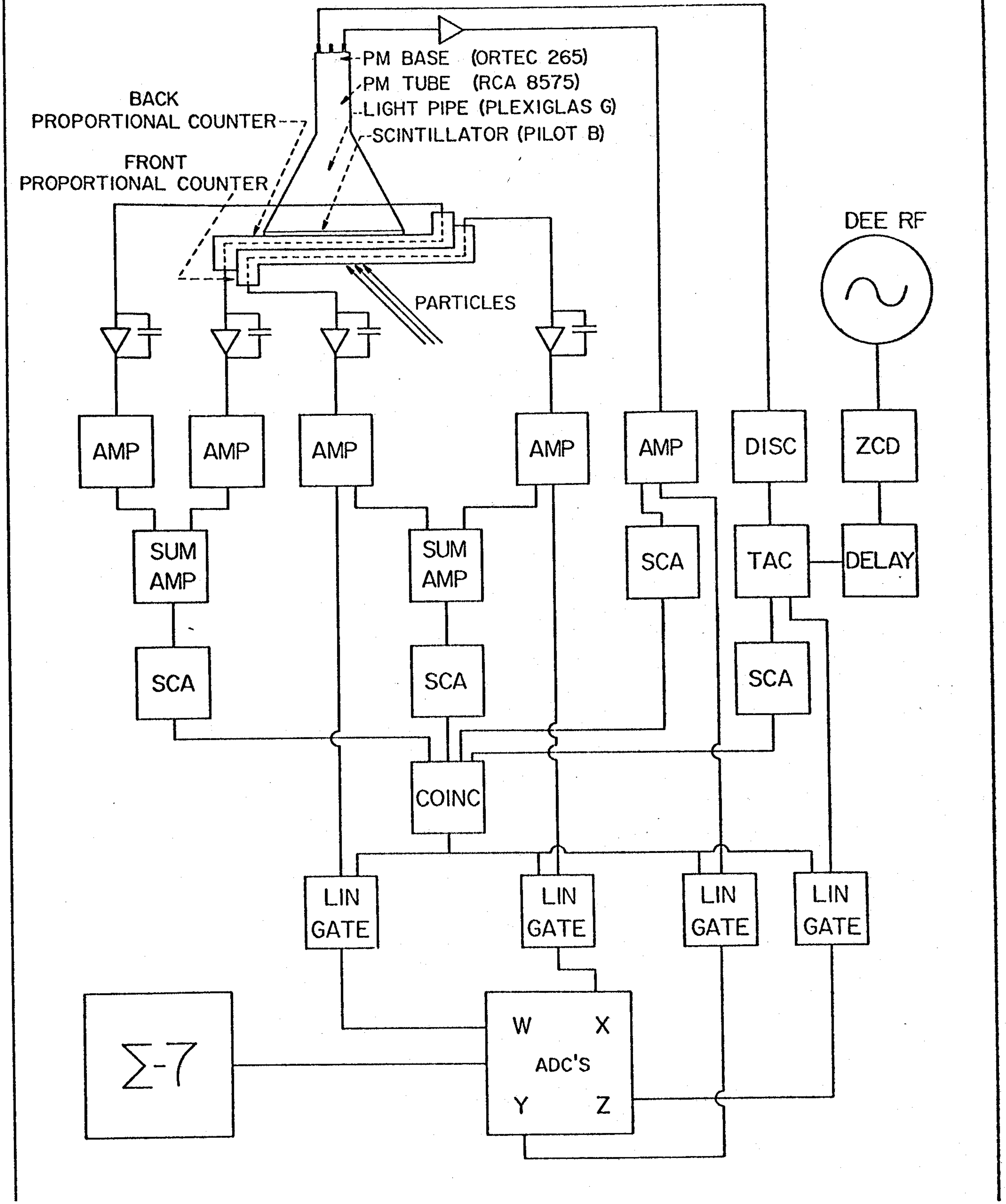

Figure 2.1.1 Block diagram of the electronics used in this detection system. Note that only the second proportional counter and the discriminator on the anode signal from the P.M. tube need be used as live gates. All other signals can be event recorded on magnetic tape.

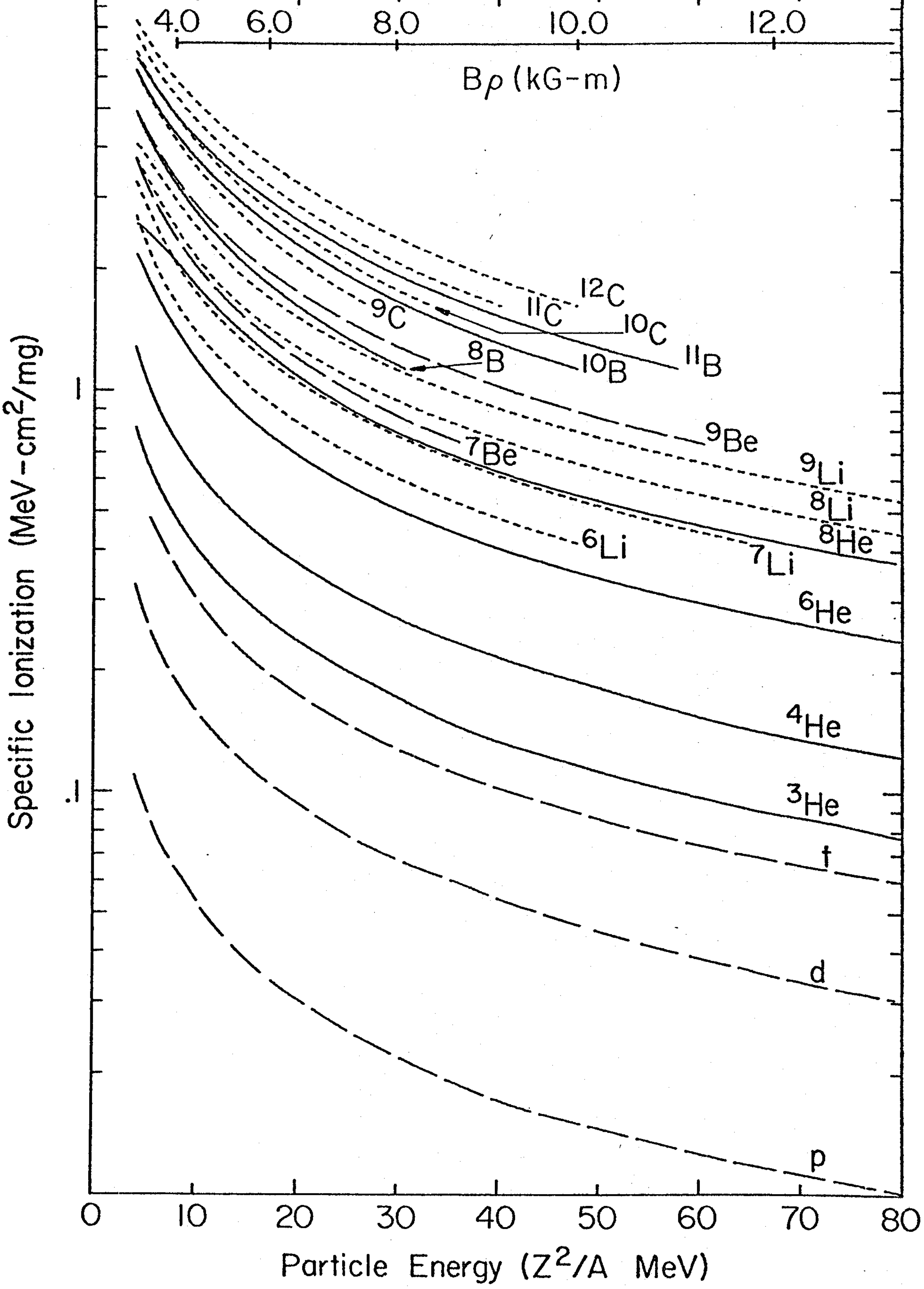

Figure 2.1.2 Specific ionization in propane versus magnetic rigidity of various ions. The values of specific ionization are from References No70 and Wi66.

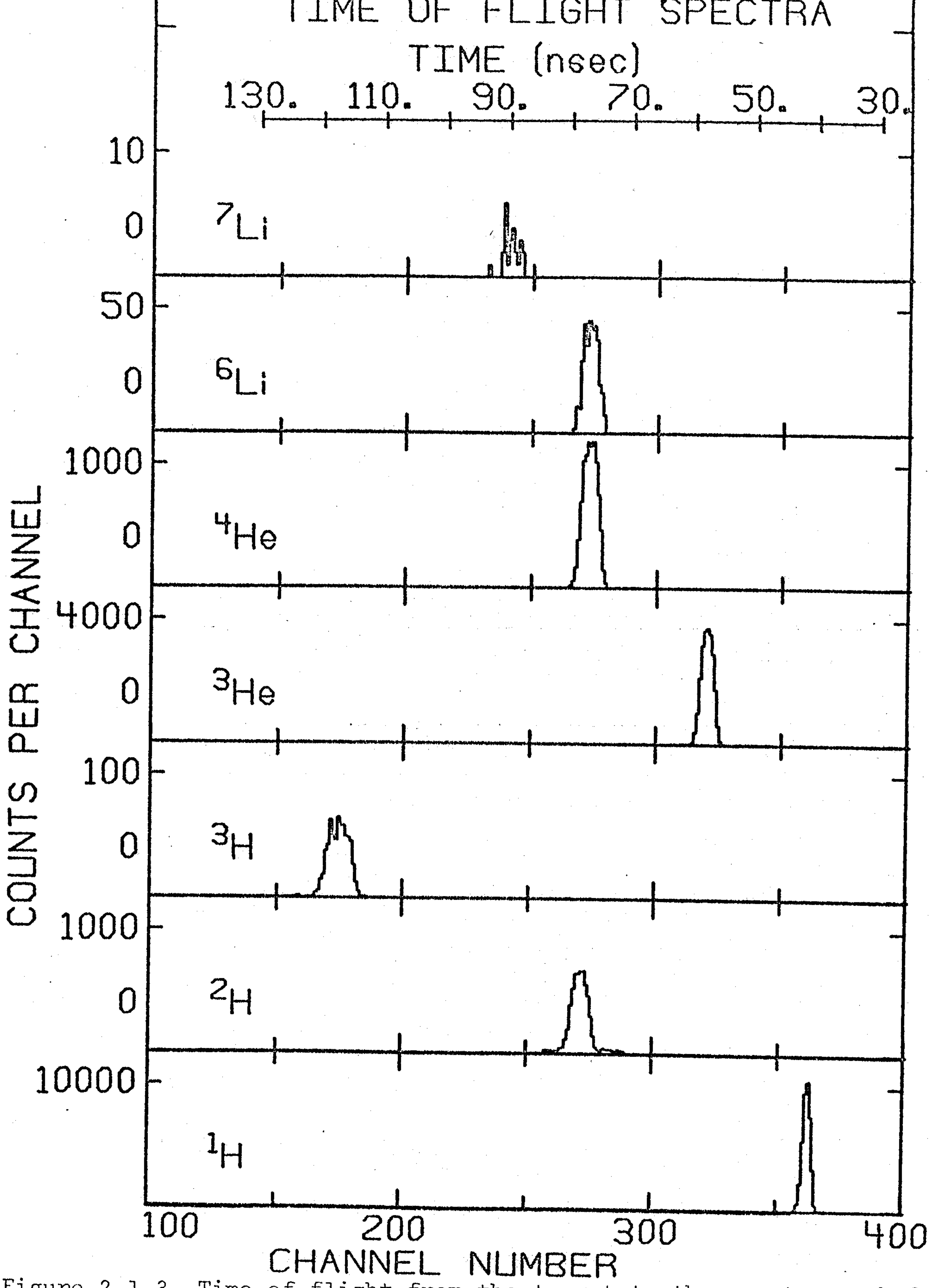

Figure 2.1.3 Time of flight from the target to the spectrograph focal plane for various ion species. The reaction products were produced by a 76.4 MeV ^{3}He beam on a ^{24}Mg target. The magnetic field was such that the ^{6}Li ions from the ground state of ^{21}Na reached the detector. Each peak represents the yield from the same amount of integrated beam current.

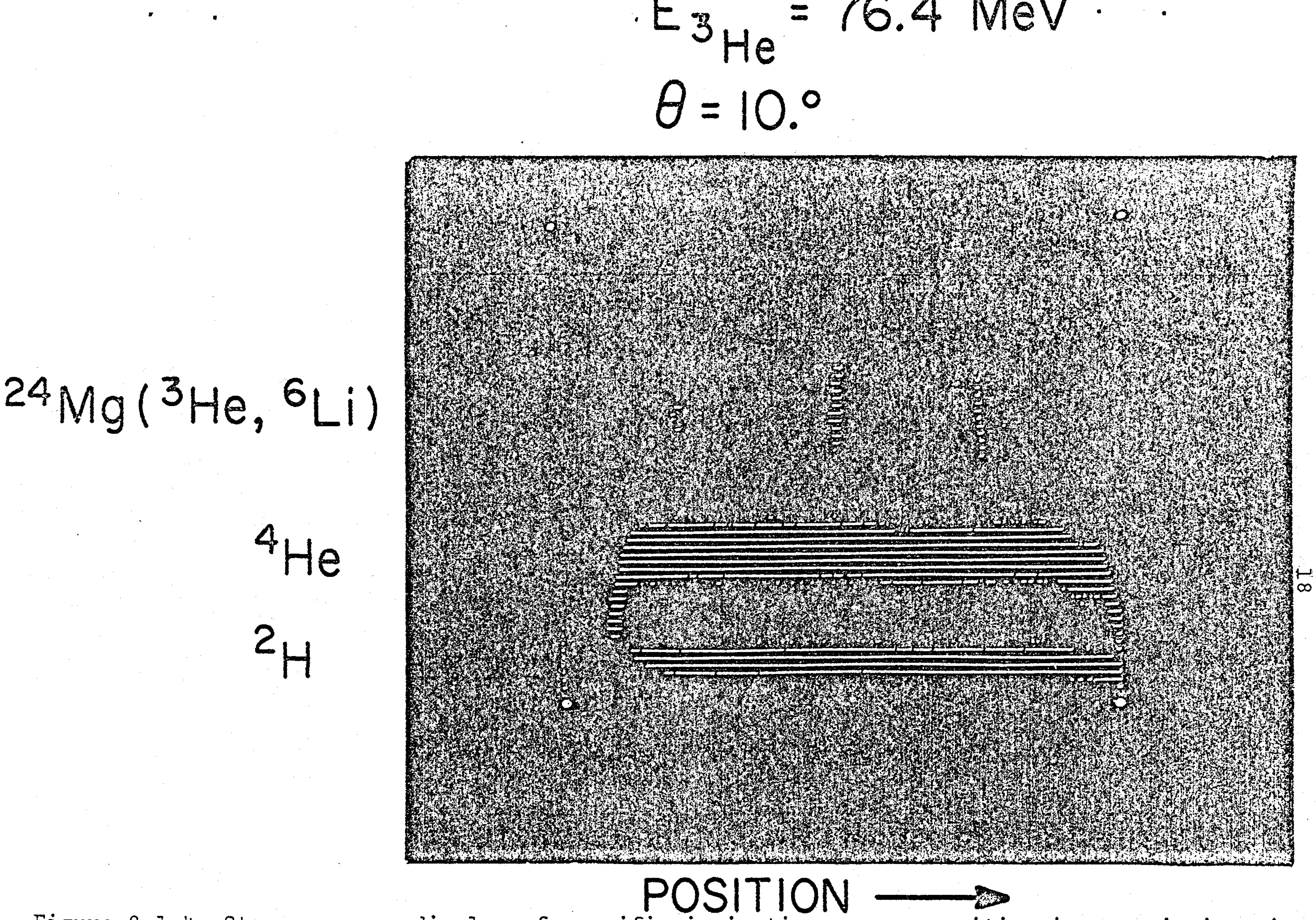

Figure 2.1.4 Storage scope display of specific ionization versus position in a resistive-wire gas-proportional counter. The particles were preselected by their time of flight through the spectrograph. Note that the specific ionization removes the ambiguity in particle identification which may arise from the time of flight.

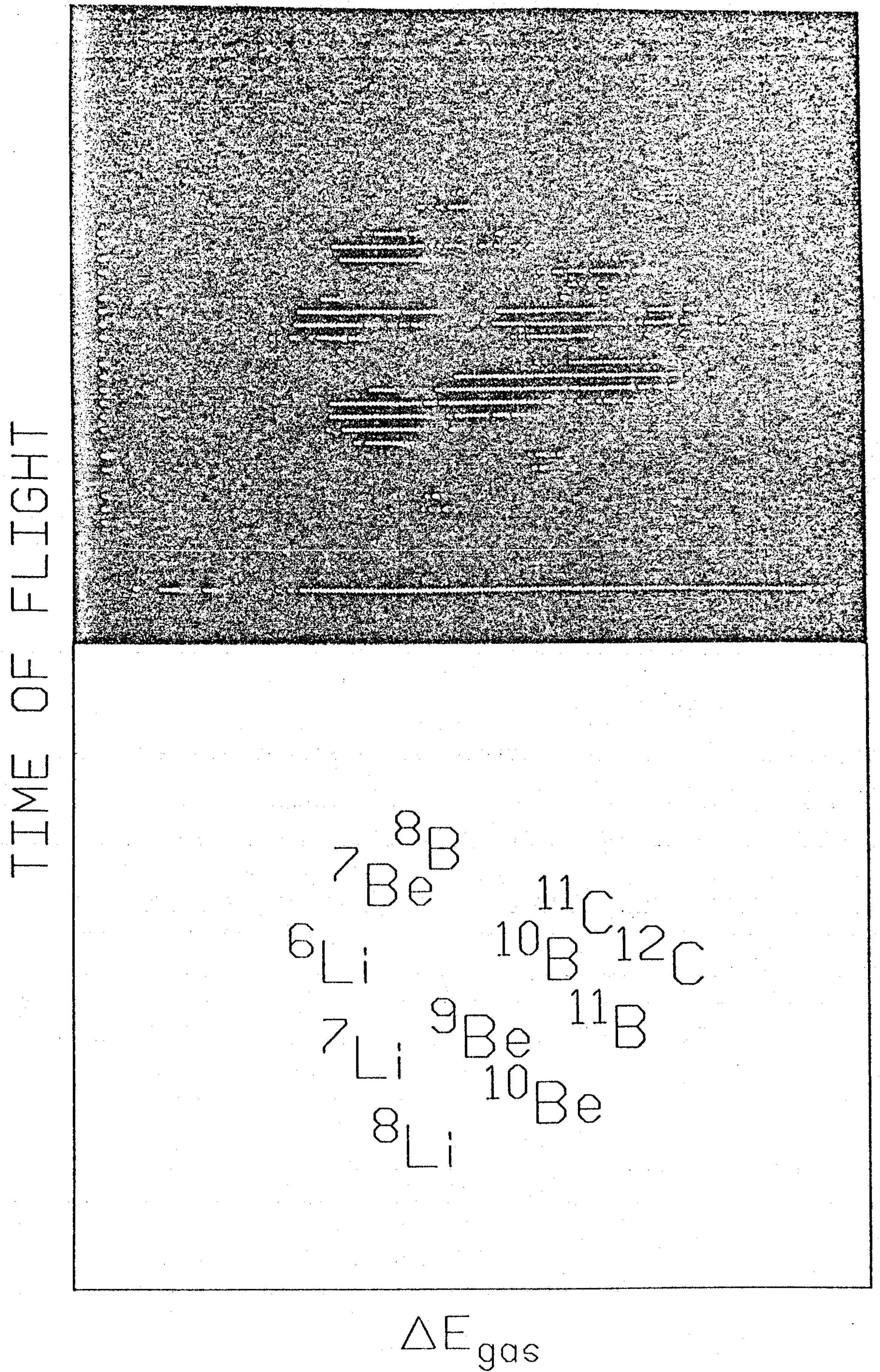

Figure 2.1.5 Storage scope display of time of flight versus energy loss in the proportional counter. The particles were produced by a 74 MeV ^{3}He beam impinged on an enriched ^{13}foil. Particles less ionizing than ^{6}Li were eliminated with an external gate.

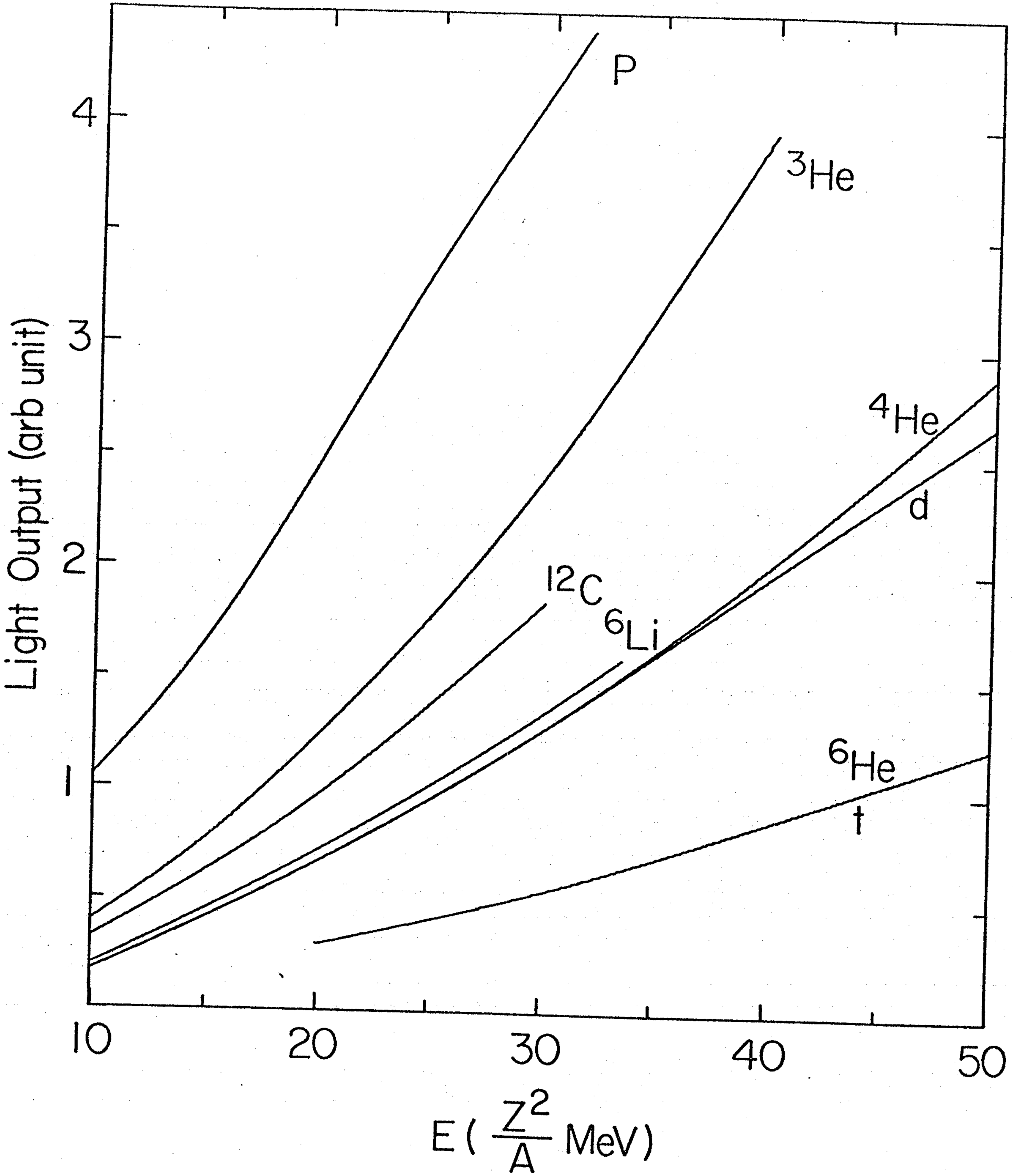

Figure 2.1.6 Light versus magnetic rigidity for particles stopped in plastic scintillator. Except for ^{6}He the curves are from Reference Be75. The ^{6}He data was taken in connection with this thesis at ^{6}He energies of 65 Z^2/A to 93 Z^2/A MeV. Also, at E ≅ 11 Z^2/A MeV, ^{9}C was found to yield one-half the light of ^{3}He and, at E ≅ 16 Z^2/A MeV, ^{8}B gave about two-thirds the light of ^{3}He.

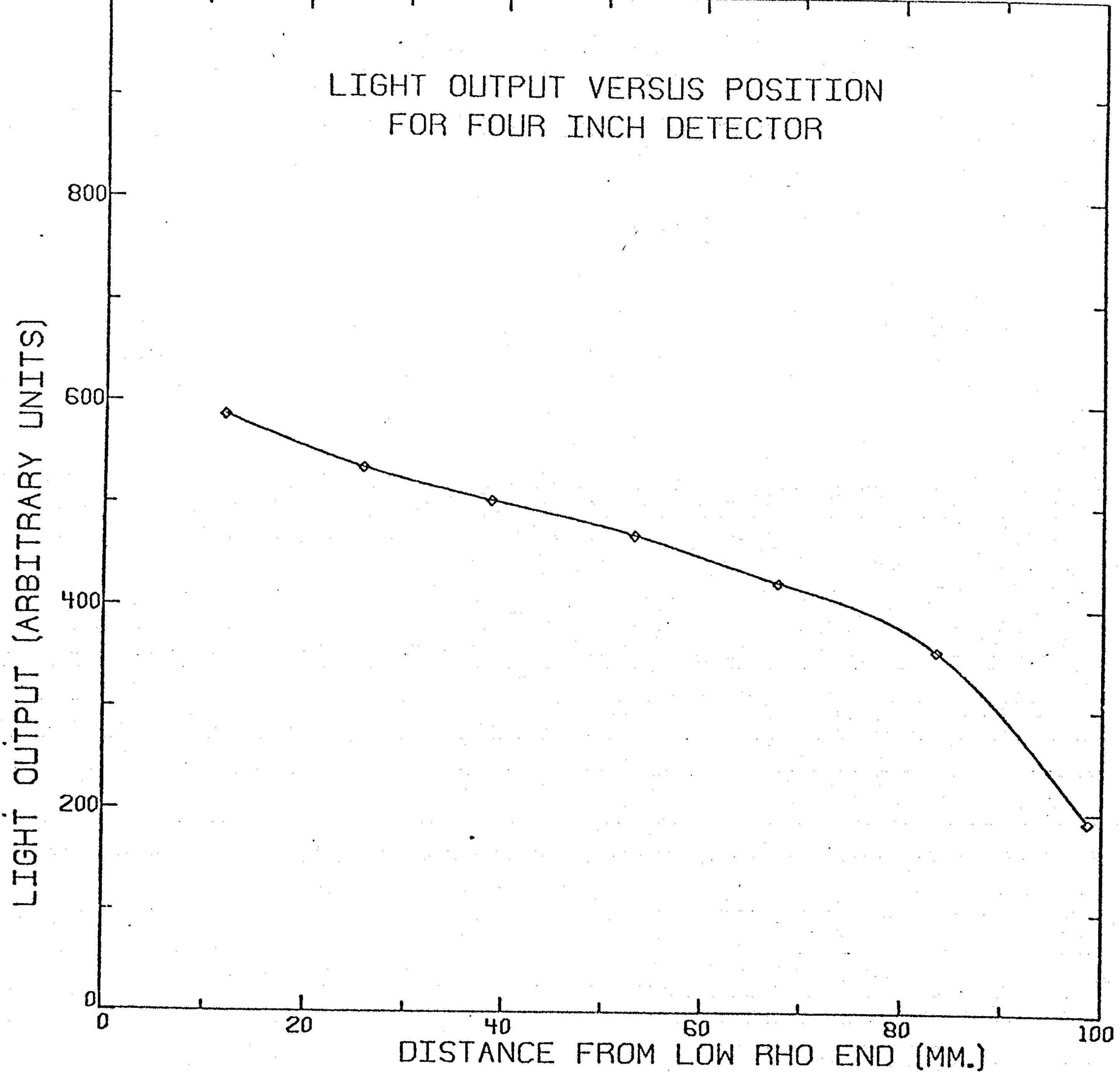

Figure 2.1.7 Light versus position for a four inch long detector. The light signal from the PM tube was found to be a function of position for various light-pipe designs.

2.2 BEAM ENERGY

The ^{3}He beam energy was measured by means of the momentum matching technique described by Trentelman and Kashy.[Tr70] The magnetic rigidity of alpha particles from the ^{27}Al(^{3}He,^{4}He) reaction was compared to the magnetic rigidity of ^{6}He particles from the ^{27}Al(^{3}He,^{6}He) reaction. The uncertainty in the beam energy deduced from this comparison is 28 keV. This uncertainty represents the sum in quadrature of 16 keV due to uncertainties in the masses,[Wa71, Ov69] 14 keV due to uncertainty in the angle and 19 keV due to the uncertainty in the relative magnetic rigidities. The latter is a result of the uncertainty in centroid determination of 4 keV for the alpha particles and 6 keV for the ^{6}He particles. Corrections were made for small changes in the beam energy due to drifts in the fields of the beam analyzing magnets. Table 2.2.1 gives the calculated beam energy and uncertainty for several sets of momentum matched reactions. The uncertainty in the beam energy magnitude implies an uncertainty of 2 keV in the mass measurements due to beam energy. The spread in beam energy accepted by the magnetic analyzing system was about 100 keV. Thus, a fluctuation of 20 keV in beam energy would affect the mass measurement by only about 7 keV.

Table 2.2.1

Incident Beam Energy and Reaction Product Momentum Bρ for Momentum-Matched Reaction Pairs at θ_L=10°

E (MeV)	dE/dθ keV/deg	Bρ Kgauss-cm	dBρ/dθ gauss-cm/deg	Reaction I	E_xI MeV	Reaction II	E_xII MeV
Protons							
14.1471(11)	8.0	449.534(27)	31	^{11}B(p,p)^{11}B	4.4451(5)	^{11}B(p,d)^{10}B	0.
16.4871(11)	10.4	548.736(21)	34	^{11}B(p,p)^{11}B	2.1247(4)	^{11}B(p,d)^{10}B	0.
18.6727(11)	12.6	626.614(18)	36	^{11}B(p,p)^{11}B	0.	^{11}B(p,d)^{10}B	0.
20.9199(20)	7.8	556.523(39)	17	^{16}O(p,p)^{16}O	6.1307(2)	^{16}O(p,d)^{15}O	0.
27.2454(21)	12.0	758.946(28)	20	^{16}O(p,p)^{16}O	0.	^{16}O(p,d)^{15}O	0.
28.9045(23)	16.4	718.093(33)	38	^{12}C(p,p)^{12}C	4.4391(3)	^{12}C(p,d)^{11}C	0.
33.0022(25)	18.9	776.813(33)	41	^{12}C(p,p)^{12}C	4.4391(3)	^{12}C(p,d)^{11}C	2.0000(5)
33.5576(23)	20.6	843.397(28)	41	^{12}C(p,p)^{12}C	0.	^{12}C(p,d)^{11}C	0.
37.6878(25)	23.2	894.755(28)	44	^{12}C(p,p)^{12}C	0.	^{12}C(p,d)^{11}C	2.0000(5)
38.7713(33)	22.5	853.017(40)	45	^{12}C(p,p)^{12}C	4.4391(3)	^{12}C(p,d)^{11}C	4.8042(12)
43.5019(34)	26.9	962.748(36)	48	^{12}C(p,p)^{12}C	0.	^{12}C(p,d)^{11}C	4.8042(12)
46.9857(37)	29.1	1001.458(38)	50	^{12}C(p,p)^{12}C	0.	^{12}C(p,d)^{11}C	6.4782(14)
50.3795(42)	31.2	1037.905(41)	52	^{12}C(p,p)^{12}C	0.	^{12}C(p,d)^{11}C	8.1045(17)
80.5579(143)	50.3	1253.520(49)	92	^{27}Al(p,α)^{24}Mg	4.1228(1)	^{27}Al(p,^{6}He)^{22}Mg	0.
86.8029(143)	55.1	1323.760(47)	96	^{27}Al(p,α)^{24}Mg	1.3659(1)	^{27}Al(p,^{6}He)^{22}Mg	0.
93.9275(144)	60.2	1387.235(45)	100	^{27}Al(p,α)^{24}Mg	0.	^{27}Al(p,^{6}He)^{22}Mg	1.2470(4)
Deuterons							
16.1938(30)	12.0	644.222(50)	65	^{16}O(d,d)^{16}O	6.1307(2)	^{16}O(d,t)^{15}O	0.
28.6829(32)	26.6	1096.203(30)	86	^{16}O(d,d)^{16}O	0.	^{16}O(d,t)^{15}O	0.
35.0181(95)	29.8	1099.145(90)	97	^{16}O(d,d)^{16}O	6.1307(2)	^{16}O(d,t)^{15}O	6.1770(30)
47.7869(99)	44.5	1418.469(70)	113	^{16}O(d,d)^{16}O	0.	^{16}O(d,t)^{15}O	6.1770(30)
63.4877(64)	84.1	1637.242(39)	241	^{12}C(d,d)^{12}C	0.	^{12}C(d,t)^{11}C	8.1045(17)
^{3}He							
69.2721(156)	71.8	1236.983(62)	124	^{27}Al(^{3}He,^{4}He)^{26}Al	3.1594(10)	^{27}Al(^{3}He,^{6}He)^{24}Al	0.
75.9213(155)	79.9	1317.227(57)	130	^{27}Al(^{3}He,^{4}He)^{26}Al	0.	^{27}Al(^{3}He,^{6}He)^{24}Al	0.

2.3 SPECTROGRAPH CALIBRATION

The momentum analyzing characteristics of the Enge 90 cm. split pole spectrograph have been calibrated for the region of the focal plane where both calibration and unknown particle groups are placed. The beam energy was adjusted for momentum matched reactions, thereby determining the magnetic rigidity ($B\rho$) of the reaction products. Then a series of other reactions were used to produce reaction products which were placed in turn at the same position on the focal plane. As the field was increased a proton NMR probe measured the magnetic field in a flat region of the spectrograph. In all the measurements a cycling procedure was used and the field set on the increasing current side of the cycle.

It was found that the magnetic field along the path responsible for the bending, $\int Bdl$, was, in spite of the recycling procedure, sensitive to the rate at which the spectrograph field energizing current was increased.[Sn67] This was ascertained by recycling and then increasing the field directly to the value where the momentum matched reactions were observed. The procedure was then repeated allowing the spectrograph to remain at several intermediate field values as the field was increased. In all this, the matched reactions insured that the beam energy and Bρ values remained unchanged. The problem was clearly the edge fields. By limiting the rate of increase of the current (15 min. from zero to 16Kg field), reproducibilities at the 1/20,000 level can be obtained on successive recyclings.[Sn67]

The magnetic rigidities of the ^{6}He particles from the calibration reactions ^{27}Al(^{3}He,^{6}He) and ^{25}Mg(^{3}He,^{6}He) are nearly the same as those of the ^{6}He particles from the reactions of interest. Therefore, only small changes in the magnetic field are necessary and these small changes imply an uncertainty in the mass measurements of less than 2 keV.

2.4 DETECTOR CALIBRATION

A resistive-wire proportional counter was used to detect the position of the reaction particles in the focal plane. The detector was calibrated by performing a least-squares fit of rho versus channel number for the alpha particles produced in the $^{12}C(^{3}He,^{4}He)$, $^{25}Mg(^{3}He,^{4}He)$ and $^{54}Fe(^{3}He,^{4}He)$ reactions. The energy levels in the residual nuclei of these reactions are well known.[Aj75,Sh76, En73, ND73] This procedure resulted in an rms deviation of about 4 keV of the observed from the accepted values for the excitation energies. The gas gain of the detector is adjusted so that the size of the signals is the same for the ^{6}He particles as for the alpha particles. This is done in order to eliminate a shift in the electronically derived position from signals of different sizes. The use of this method of calibration resulted in uncertainties in the excitation energies of about 2 keV per MeV of excitation energy due to different calibrations used. This uncertainty is added in quadrature to the uncertainty of 3 keV from the residuals and the uncertainty of 2 to 20 keV in the centroid determination for the low cross-section $(^{3}He,^{6}He)$ reactions.

2.5 TARGET THICKNESS MEASUREMENTS

The mass measurement of the $4n+3, T_z = -1/2$ nuclei has been made on two sets of targets. The first set, with the exception of the ^{50}Cr target, consisted of 259 to 324 μg/cm^2 carbon backings. The thickness of the self-supported foils was measured by means of the energy loss of 5.48 MeV alpha particles from ^{241}Am. The energy of the alpha particles was measured in a surface barrier silicon detector. The thickness of the carbon-backed targets was measured by means of the energy loss of 56 MeV ^6Li particles from the $^{12}C(^3He,^6Li)$ reaction. A 217±22 μg/cm^2 carbon foil was employed to measure the cross-section for this reaction of 130±17μg/sr at $\theta_{Lab} = 10^\circ$. The spectrograph was used to measure the energy of the ^6Li ions. The targets were rotated so that the carbon backing faced either towards or away from the spectrograph aperature. The difference in the observed energy of the ^6Li particles for the two target orientations is just the ^6Li energy loss in the metal target. The size of the ^6Li energy loss was 12. to 27. keV. The specific ionization of 56 MeV ^6Li particles is about twice that for 52. MeV ^6He particles.[No70] Hence, use of the ^6Li energy loss should yield an accurate determination for the ^6He energy loss in the targets. The thickness of the carbon backings was determined by measuring the relative yields of ^{6}Li particles from the backings and from a thick carbon foil, as well as the energy loss of the ^{6}Li ions in the backings and in the thick foil. The thickness of the backings ranged from 26 to 47 μg/cm^{2}. Table 2.5.1 shows the thickness, method of measurement and energy-loss corrections of the targets. Notice that these small energy-loss corrections imply only very small (less than 4 keV) uncertainties in the mass measurements.

Table 2.5.1 Target Thickness

Frame Number	Isotope	Thickness ($\mu g/cm^2$)[a]		Energy Loss (keV)[b]		Method[c]	% Enrichment
		Target	Backing	^{6}He	^{3}He		
428	^{27}Al	259	---	20.	9.	α E loss	100
155	^{46}Ti	290	---	20.	9.	α E loss	83.8
325	^{54}Fe	289	---	19.	9.	α E loss	96.66(33)
378	^{58}Ni	324	---	21.	10.	α E loss	99.89(1)
426	^{50}Cr	87	61	5.7	7.6	α E loss	96.80(5)
426	^{50}Cr[d]	82	47	5.5	6.3	^{6}Li E loss	96.80(5)
227	^{25}Mg	61	30	4.8	4.6	^{6}Li E loss	99.21(5)
207	^{58}Ni	89	37	6.0	5.5	^{6}Li E loss	99.890
632	^{46}Ti	40	27	2.9	3.5	^{6}Li E loss	81.2
634	^{54}Fe	99	31	6.6	5.5	^{6}Li E loss	96.81(5)
627	^{27}Al	62	27	4.8	4.4	^{6}Li E loss	100

---

a) The uncertainty in the thicknesses are 10% for the target and 15% for the backing.

b) The energy loss for ^{6}He is that of 52 MeV ^{6}He particles in one half the target thickness, while for ^{3}He, the energy loss is that for 70 MeV ^{3}He particles in one half the target thickness plus that in the backing.

c) For those targets measured by means of ^{6}Li energy loss, the measurement of thickness of the backings also employed the relative yields from the ^{12}C(^{3}He,^{6}Li) reaction.

d) Only the thickness of the ^{50}Cr target was accurately measured by both methods.

3 EXPERIMENTAL RESULTS

3.1 MASS MEASUREMENTS AND SPECTRA

The mass excess of ^{43}Ti, ^{47}Cr, ^{51}Fe and ^{55}Ni have been remeasured by the method described and have been found to be consistent with the results of Mueller *et al.*[Mu75] The recent measurement employed thin targets evaporated on carbon foils. The target thicknesses were measured by means of the energy loss of ^{6}Li ions from the ^{12}C(^{3}He,^{6}Li) reaction induced in the backings. Tables 3.1.1 and 3.1.2 contain the results of the recent measurements and those of Mueller *et al*. The recent measurement employed thinner targets than previously and also made use of a second calibration reaction ^{25}Mg(^{3}He,^{6}He) as well as the ^{27}Al(^{3}He,^{6}He) reaction used previously. The magnetic rigidity of the ^{6}He particles from the ^{25}Mg(^{3}He,^{6}He) reaction leaving ^{22}Mg in its first excited state have nearly the same magnetic rigidity as those from the ^{58}Ni(^{3}He,^{6}He) reaction leaving ^{55}Ni in its ground state. The two calibrations gave consistent results. Table 3.1.3 shows the error analysis for a single measurement. Repeated measurements reduce the random errors due to most sources except those from the uncertainties in calibration Q-value and target-thickness corrections. The recent measurements increase the reliability of the values for the mass excesses since a different calibration and thinner targets were employed. In the case of ^{47}Cr, the uncertainty in the mass excess of the $3/2^-$ ground state is greatly reduced since it has been resolved from the $5/2^-$ and $7/2^-$ states. During the analysis of this data, a discrepency from the Mass 71 value^{Wa71}for the mass of ^{57}Ni was observed. Appendix B discusses the result of the measurement of the mass of ^{57}Ni via the ^{58}Ni(^{3}He,^{4}He) reaction which removed the discrepency.

Figures 3.1.1 to 3.1.4 show spectra of the ^{6}He particles taken at laboratory angles of from 4.5 to 27 degrees. Targets of approximately 1 mg/cm^2 self-supporting metal foils and a solid angle of 1.2 msr. were employed in the acquisition of these spectra which are normalized to represent the yield from 10 millicoulombs of integrated beam current. The resolution in these spectra is limited by energy loss in the targets to greater than 70 keV. The three most prominent peaks in the spectrum of each nucleus have been identified by comparison with the mirror nuclei as the lowest lying $7/2^-$, $3/2^+$ and $1/2^+$ states. Thin targets were employed to obtain the high resolution shown in Figures 3.1.5 through 3.1.7. These spectra indicate several levels that were not resolved in the thick target data. Of particular interest are the three lowest lying states in ^{47}Cr. The previously large uncertainty in the ground state mass of ^{47}Cr resulted from the inability to resolve these states. This uncertainty has now been resolved. Tables 3.1.4 through 3.1.7 list the excitation energies of levels in ^{43}Ti, ^{47}Cr, ^{51}Fe and ^{55}Ni which have cross-sections of greater than about 60 nb/sr at $\theta_{Lab} = 10^{o}$. Levels with smaller cross sections are listed if the thick target data verifies their observation.

Table 3.1.1 Mass Excess (MeV)

Nucleus	Previous[a]	Present	Average
^{43}Ti	-29.328±0.012	-29.305±0.014	-29.319±0.008[b]
^{47}Cr(g.s.)	-34.608±0.040[c]	-34.553±0.015	-34.561±0.012[d]
$(7/2^-)$	-34.386±0.012	-34.371±0.013	-34.379±0.0010
^{51}Fe(g.s.)	-40.219±0.017	-40.200±0.015	-40.201±0.012[d]
$(7/2^-)$	-39.940±0.013	-39.938±0.013	-39.939±0.0010
^{55}Ni	-45.337±0.011[e]	-45.327±0.013	-45.333±0.0010

a) Reference Mu75

b) The average mass excess of ^{43}Ti includes the measurement of Ref. Al67. (-29.321±0.010 MeV)

c) In the measurement of Mueller *et al.*, the ^{47}Cr g.s. was not resolved. The separation of the $7/2^-$ and the ground state was taken from the present measurements.

d) The relative exitation of the $7/2^-$ and $5/2^-$ ground state from the present measurement was employed to deduce the ^{51}Fe and ^{47}Cr ground state masses.

e) This value represents an 8.2 keV increase in the mass of ^{55}Ni from the value of Mueller *et al.*[Mu75] due to the measurement of the ^{58}Ni mass of Jolivette *et al.*[Jo74]

Table 3.1.2 Reaction Q-Values

Reaction	Q-Value (MeV) Previous[a]	Q-Value (MeV) Present[b]
^{46}Ti(^{3}He,^{6}He)^{43}Ti	-17.463±0.012	-17.486±0.014
^{50}Cr(^{3}He,^{6}He)^{47}Cr(g.s.)	-18,313±0.040	-18.368±0.014
(7/2^{-})	-18.535±0.012	-18.550±0.013
^{54}Fe(^{3}He,^{6}He)^{51}Fe(g.s.)	-18.698±0.017	-18.697±0.015
(7/2^{-})	-18.969±0.013	-18.971±0.013
^{58}Ni(^{3}He^{6}He)^{55}Ni	-17.555±0.011	-17.565±0.013

a) Reference Mu75

b) Q-Values measured relative to the ^{27}Al(^{3}He,^{6}He)^{24}Al(g.s.) and ^{25}Mg(^{3}He,^{6}He)^{24}Mg(3.3082 reaction Q-Values of -19.812±0.003 MeV[Ov69,Wa71] and -18.7656±0.004 MeV[No74,Ha74,Wa71,En73] respectively.

Table 3.1.3 Error Analysis

Parameter	Uncertainty	Effect on $^{58}Ni(^{3}He,^{6}He)^{55}Ni$ Q-Value (keV)
1. Beam Energy (absolute)	38 keV	2.0
2. Beam Energy (fluctuation)	20 keV	7.0
3. Detection angle	.2°	8.0
4. Angular yield dependence	.25°	5.0
5. Peak Centroid	.3 ch	3.3
6. ^{24}Al mass[a]	3 keV	3.0
7. Target thickness	10%	1.2
8. B-field scaling		<1.0
9. B-field reproducibility	1/20,000	field not changed
10. Detector Calibration and linearity		4.0
	Overall uncertainty	13.5

a) Reference Ov 69

Table 3.1.4 ^{43}Ti Energy Levels

Ex(MeV)	Uncertainty (keV)	J^{π}
0.0	0.	$7/2^{-}$
0.319	6.	$3/2^{+}$
0.475	10.	
0.998	10.	$1/2^{+}$
1.16	10.	
1.47	10.	
1.80	15.	
2.25	10.	
2.438	9.	
2.99	15.	

Table 3.1.5 ^{47}Cr Energy Levels

Ex(MeV)	Uncertainty(keV)	J^{π}
0.0	0	$3/2^-$
0.102	10	$5/2^-$
0.182	7	$7/2^-$
0.478	7	$3/2^+$
0.890	20	
1.355	8	
1.451	9	
1.541	15	
1.831	8	$1/2^+$
2.131	9	
2.406	10	
2.557	10	
2.609	10	
2.661	10	
2.848	10	
3.430	10	
3.504	11	
3.747	11	
4.169	12	
4.295	12	
5.409	15	

Table 3.1.6 ^{51}Fe Energy Levels

Ex(MeV)	Uncertainty (keV)	J^{π}
0.0	0	$5/2^-$
0.262	6	$7/2^-$
1.218	10	
1.525	9	
1.866	13	
2.063	7	$3/2^+$
2.489	8	$1/2^+$
3.013	9	
3.127	9	
3.310	10.	
3.964	12.	(doublet)
4.456	13.	

Table 3.1.7 ^{55}Ni Energy Levels

Ex(MeV)	Uncertainty (keV)	J^{π}
0.0	0	$7/2^-$
2.089	6	
2.462	5	
2.839	5	
2.888	7	
3.185	6	$1/2^+$
3.502	15	
3.592	15	
3.752	7	$3/2^+$
3.784	15	
4.046	9	
4.444	10	(doublet)
4.616	11	
4.743	12	
4.983	11	
5.178	11	
5.389	12	
5.876	13	
5.937	13	
6.60	50	
6.87	50	

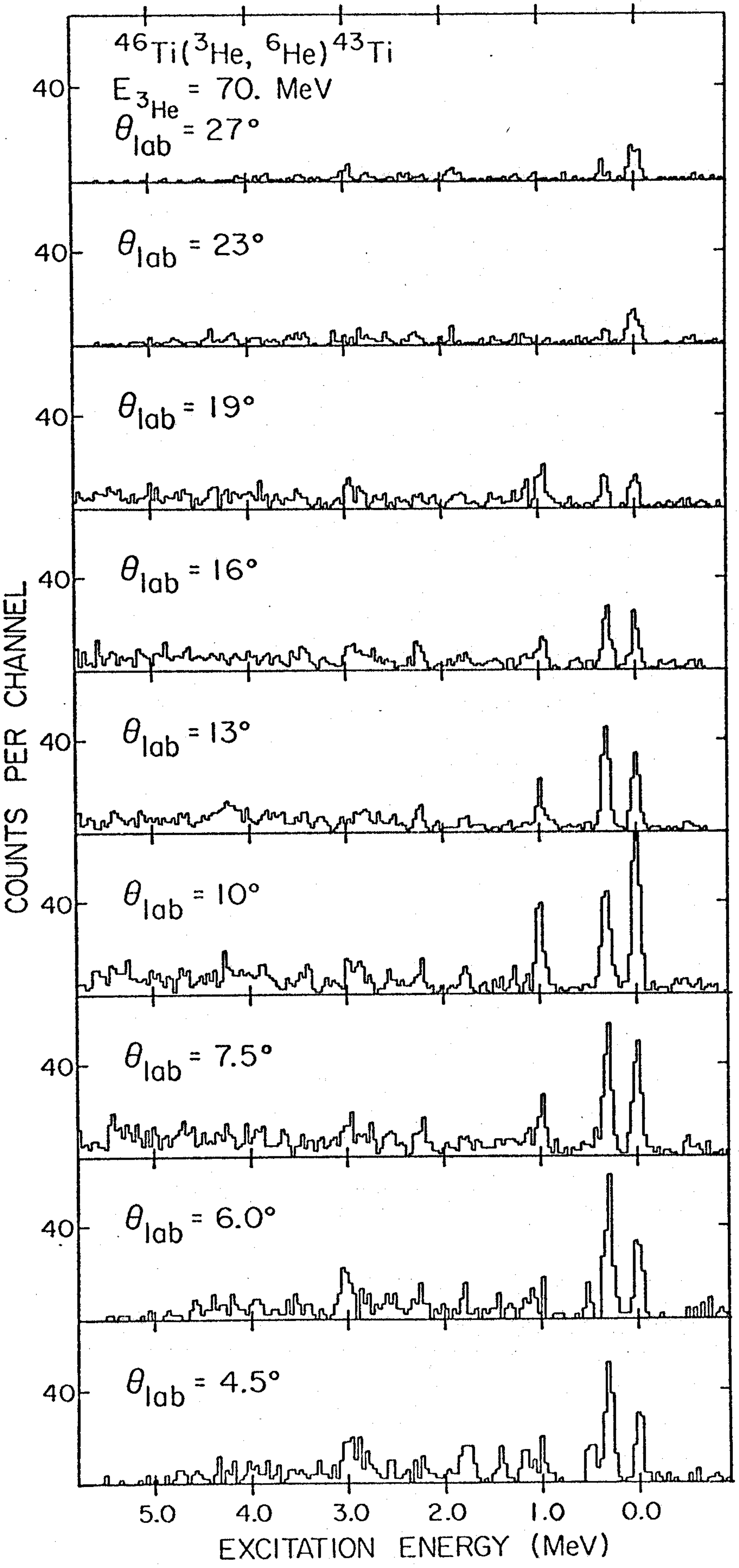

Figure 3.1.1 Spectra of ^{6}He particles. A 1 µg/cm^2 thick self-supporting 85% isotopically enriched ^{46}Ti foil was employed. The yields have been normalized to represent the same solid angle and charge for each spectrum. The three strong states have been identified as the J^π = 7/2−, 3/2+, and 1/2+ levels at 0.0, 0.319 and 0.998 MeV excitation respectively.

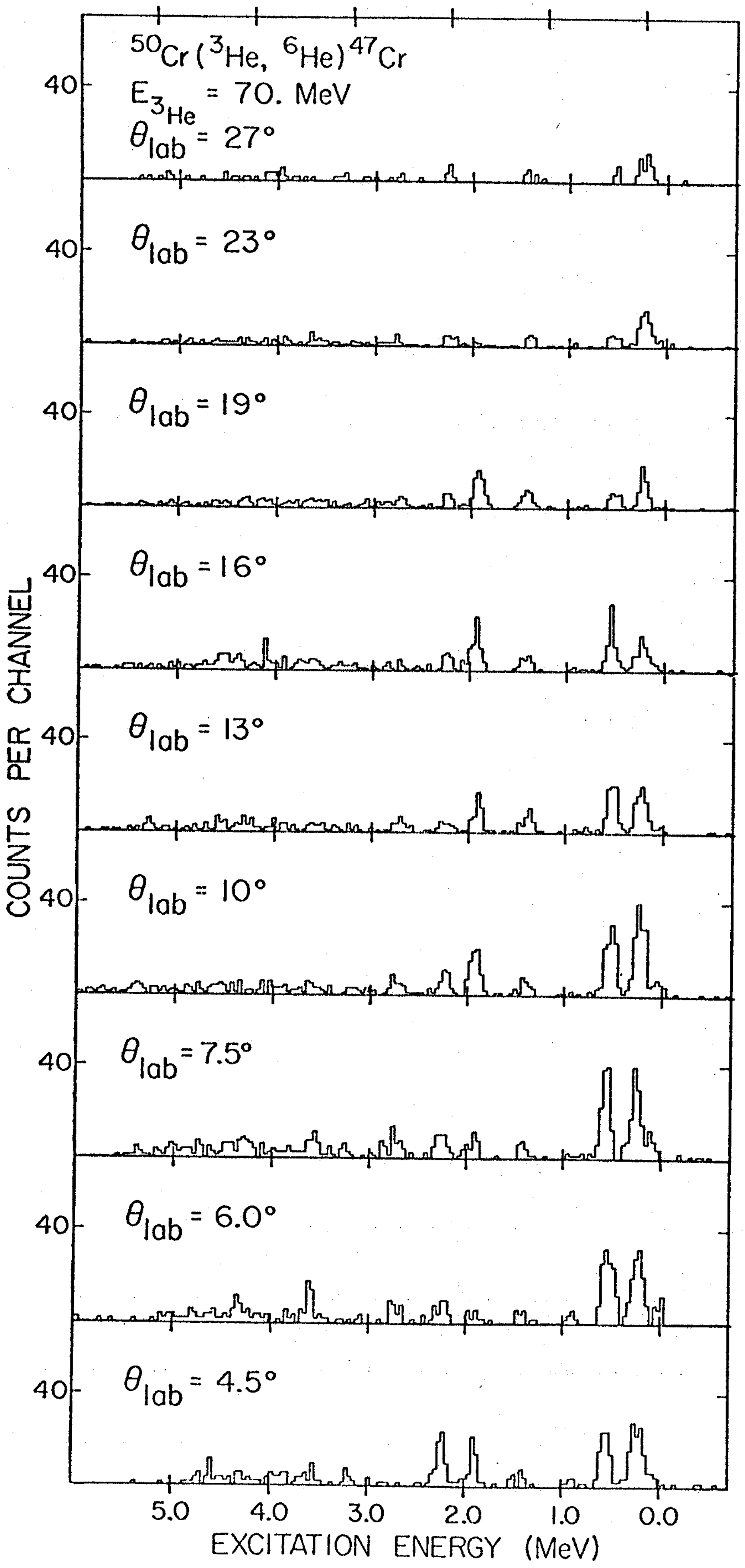

Figure 3/12 spectra of ^{6}He particles. A 1 μg/cm^{2} thick self-supporting 97% isotopically enriched ^{50}Cr foil was employed. The yields have been normalized to represent the same solid angle and charge for each spectrum. The three strong states have been identified as the $J^{\pi} = 7/2^{-}$, $3/2^{+}$ and $1/2^{+}$ levels at 0.182, 0.478 and 1.831 MeV excitation respectively.

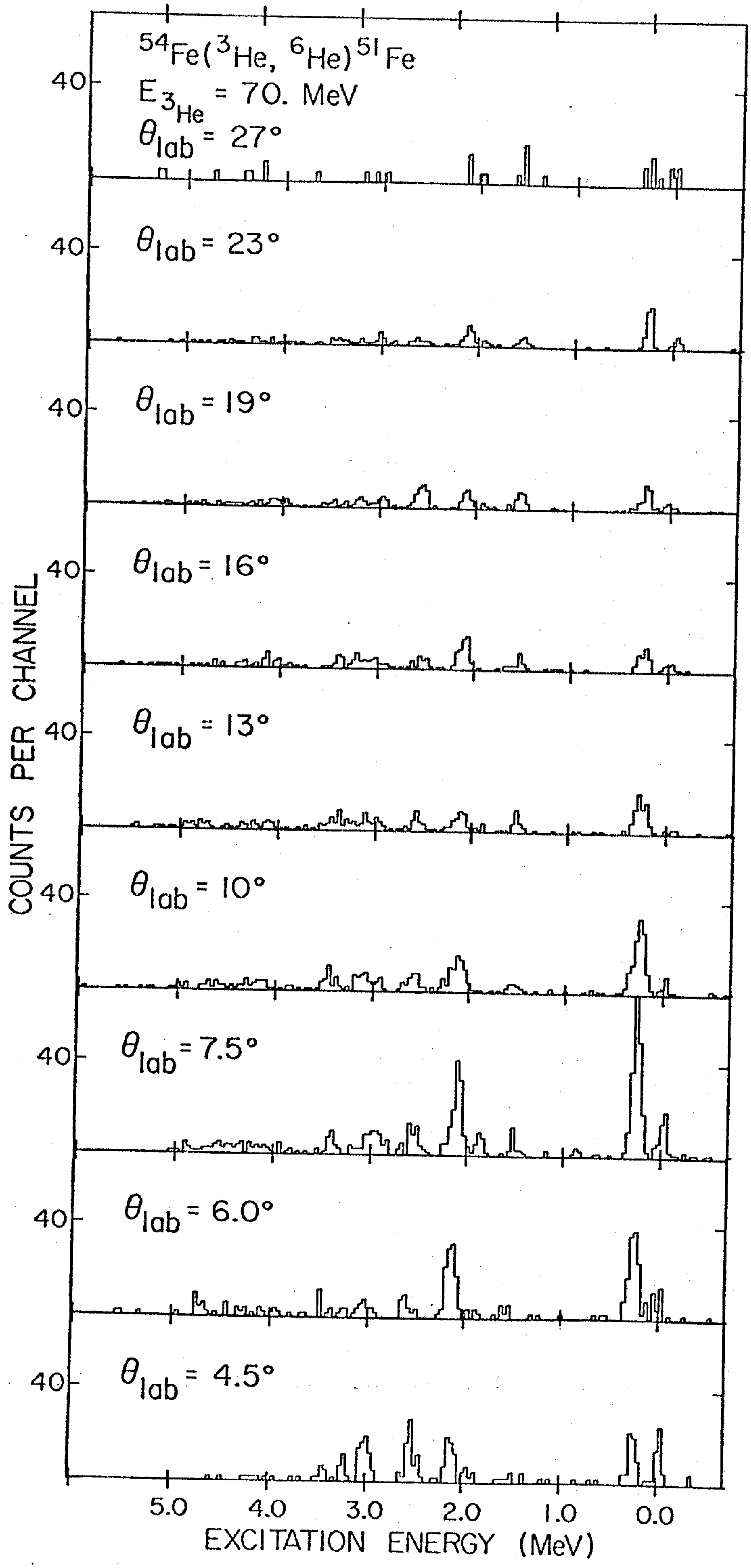

Figure 3.1.3 spectra of ^{6}He particles. A 1 μg/cm^2 thick self-supporting 97% isotopically enriched ^{54}Fe foil was employed. The yields have been normalized to represent the same solid angle and charge for each angle. The three strong states have been identified as the Jπ = 7/2$^-$, 3/2$^+$, and 1/2$^+$ levels at 0.262, 2.063 and 2.489 MeV excitation respectively.

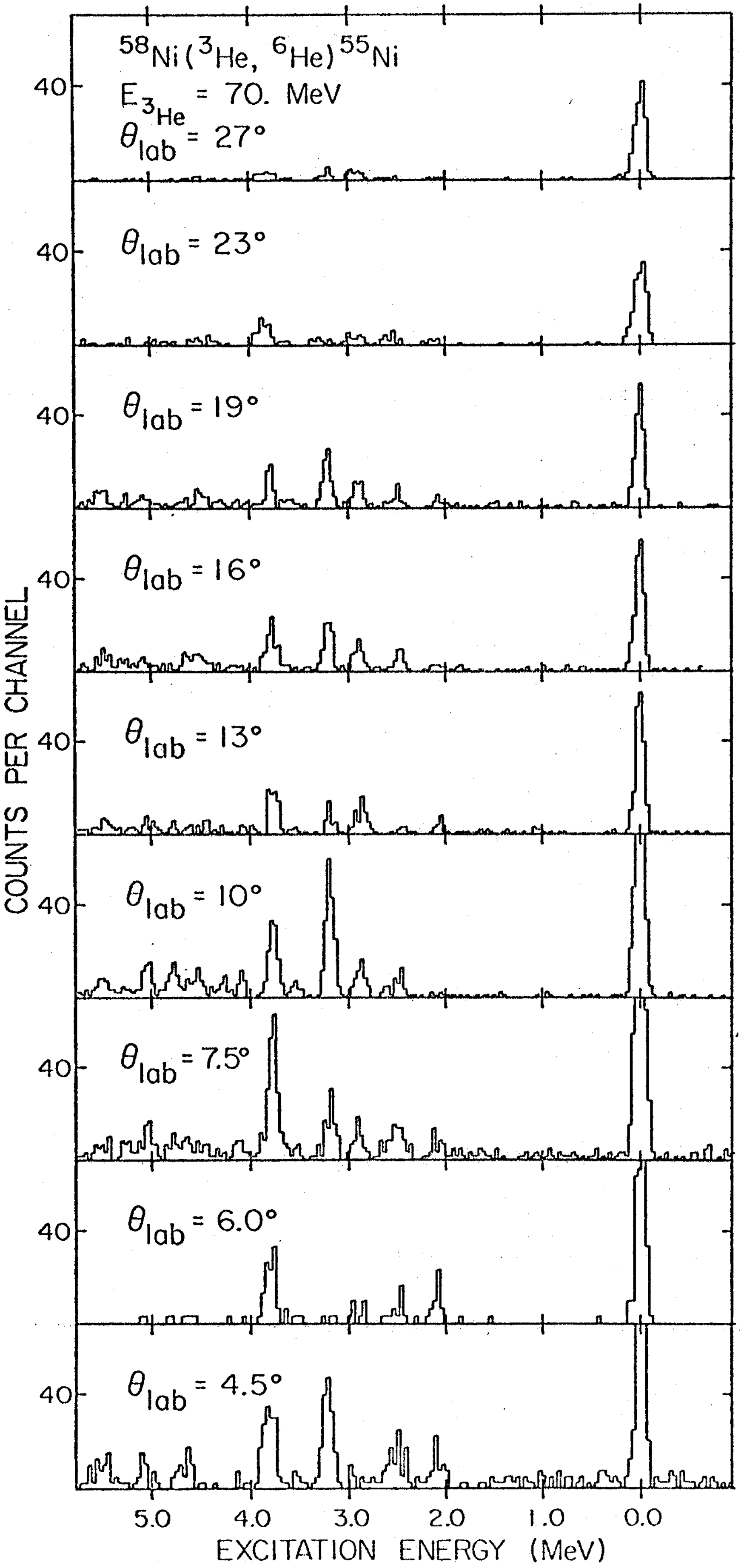

Figure 3.1.4 Spectra of ^{6}He particles. a 1.2 μg/cm^2 thick self-supporting 99.9% [illegible] isotopically enriched ^{58}Ni foil was employed. The yields have been normalized to represent the same solid angle and charge for each spectrum. The three strong states have been identified as the $J^\pi = 7/2^-$, $3/2^+$ and $1/2^+$ levels at 0.0, 3.752 and 3.185 MeV excitation respectively.

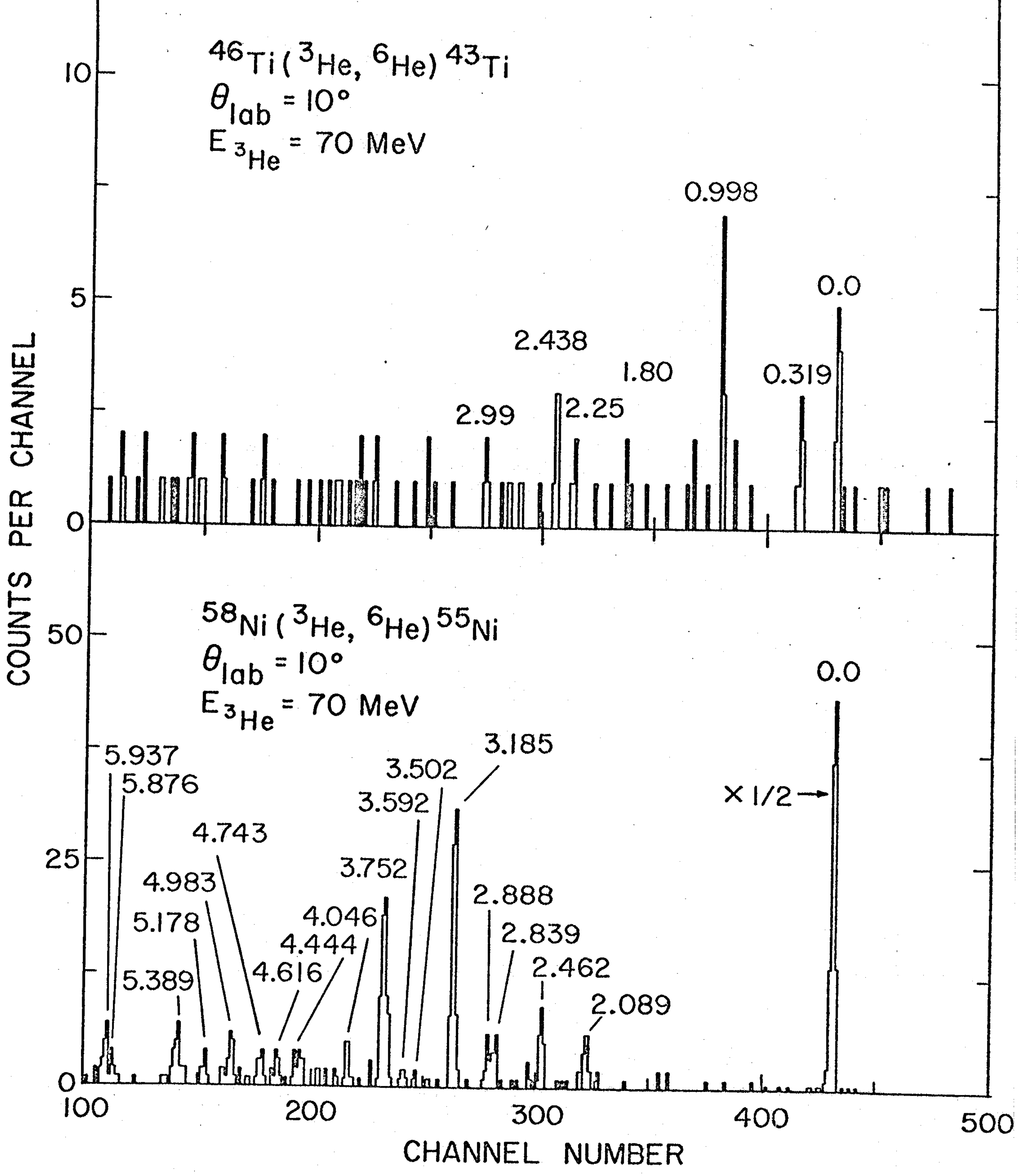

Figure 3.1.5 High resolution spectra of ^{46}Ti(^{3}He,^{6}He) and ^{58}Ni(^{3}He,^{6}He) reactions. The observed resolution is about 30 keV FWHM.

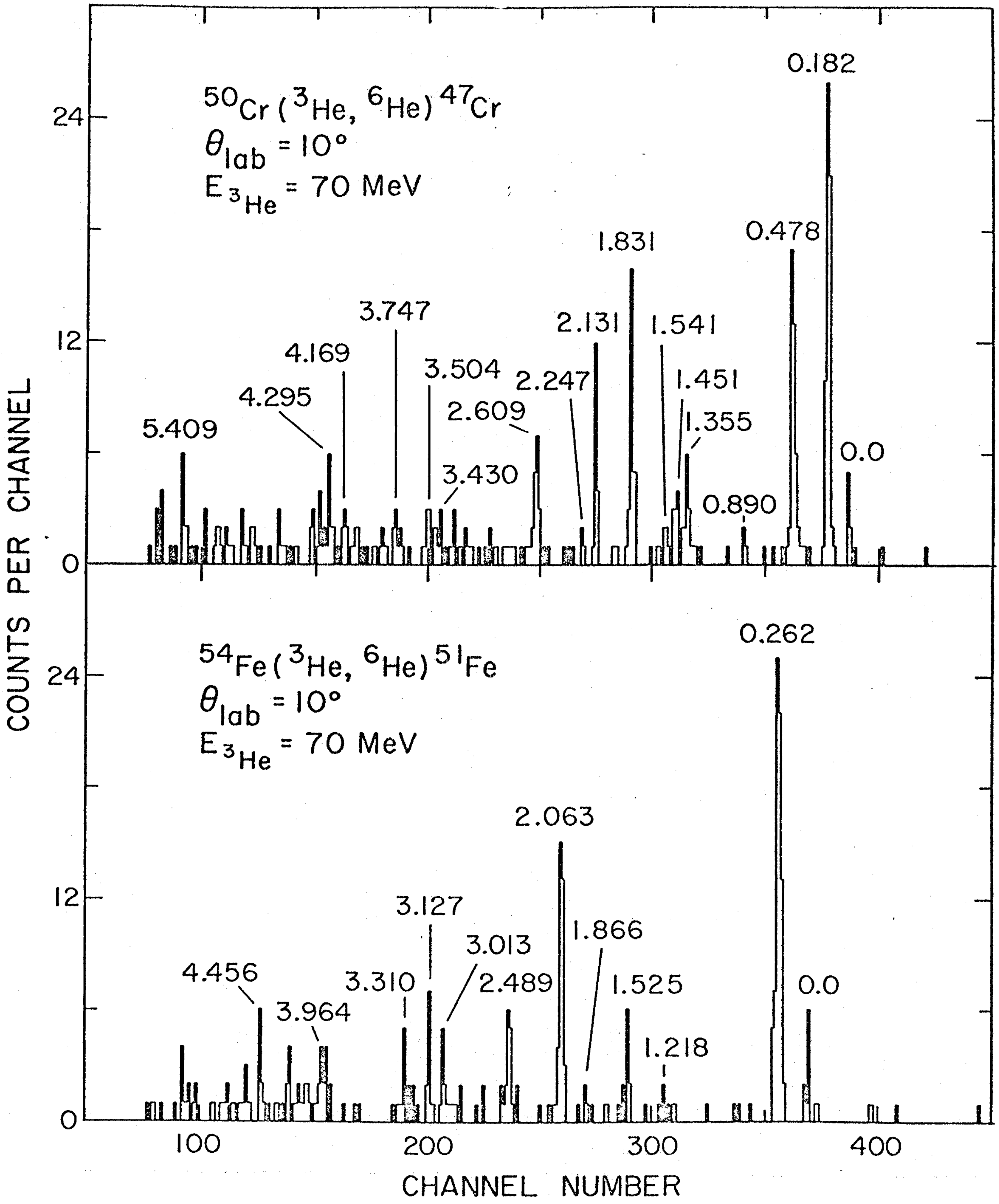

Figure 3.1.6 High resolution spectra of ^{50}Cr(^{3}He,^{6}He) and ^{54}Fe(^{3}He,^{6}He) reactions. The observed resolution is about 35 keV FWHM.

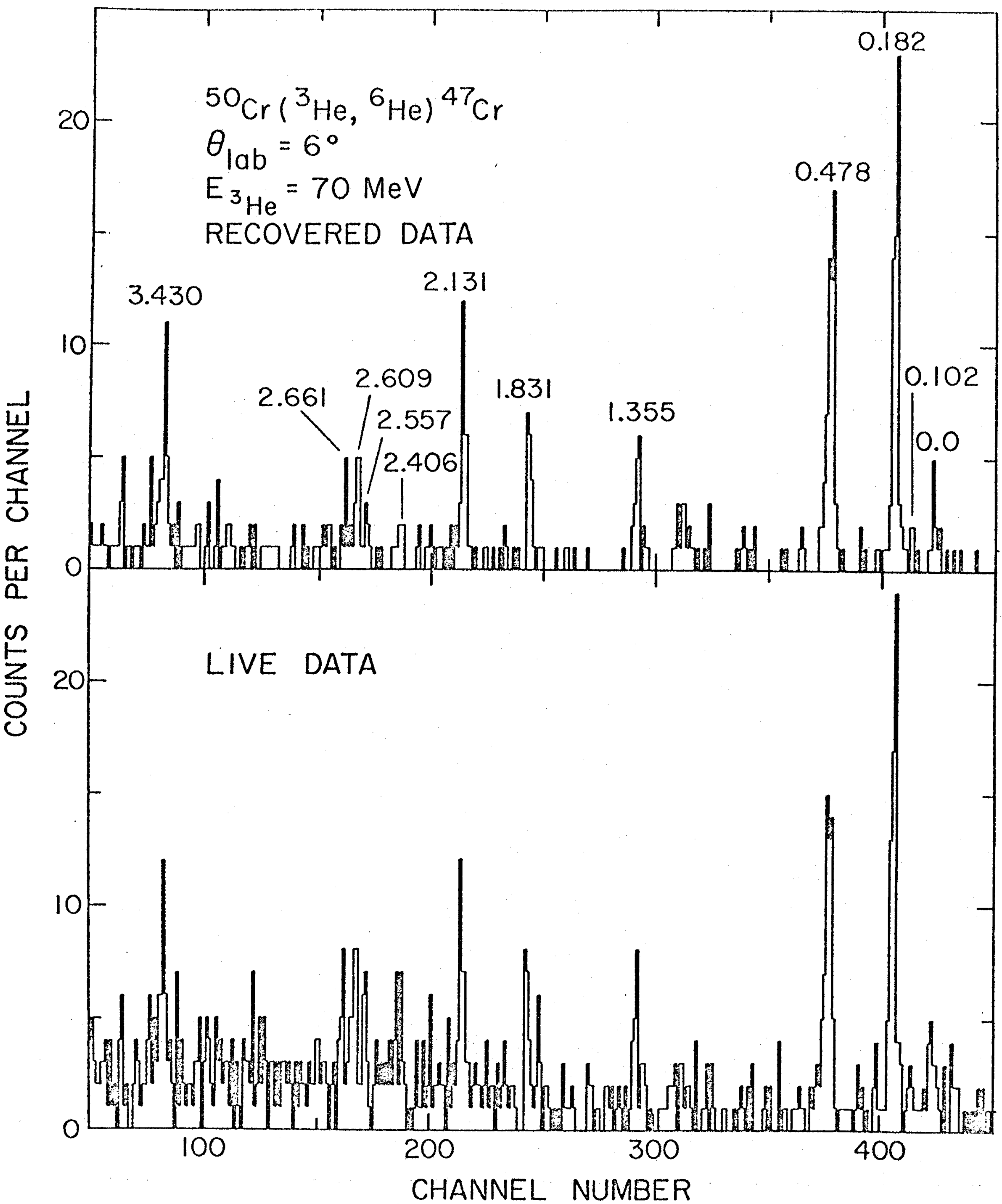

Figure 3.1.7 Spectra of $^{50}Cr(^3He,^6He)$ reaction. This illustrates how well the data may be cleaned of background events by employing event recording. The apparent peaks in about channels 250 and 430 in the live data spectrum are alpha particles that were misidentified and later correctly eliminated during the play back of the tape.

3.2 ANGULAR DISTRIBUTIONS

Angular distributions of the (^{3}He,^{6}He) reaction have been taken on 1 mg/cm^2 ^{46}Ti, ^{50}Cr, ^{54}Fe, and ^{58}Ni targets from 4.5° to 27° in the laboratory. The results have been compared empirically with those of Nann *et al.*[Na76], who measured the angular distributions of the 7/2$^-$, 3/2$^+$ and 1/2$^+$ levels excited in the ^{42}Ca(^{3}He,^{6}He)^{39}Ca reaction. Figure 3.2.1 shows the angular distributions of the present work together with those of Nann *et al.* The line in each distribution is a smooth curve drawn to guide the eye and represents an average of the Ni and Ca shapes for each spin and parity. The data for the 7/2$^-$ levels follows the empirically determined curves well. The structure in the data for the 7/2$^-$ level in Cr is not as pronounced as for the other nuclei. This is at least partially due to the presence of the unresolved 5/2$^-$ state. The Fe data (see Figure 3.1.3) indicates that at 4.5 degrees the 5/2$^-$ level should have a yield comparable to that of the 7/2$^-$ level. The 3/2$^+$ levels are all well resolved and all have similar angular distributions. The 1/2$^+$ levels exhibit more structure in their angular distributions than the 7/2$^-$ and 3/2$^+$ levels and the shapes of these angular distributions vary. However, the angular distributions of the $1/2^+$ levels all have minima at approximately 6 and 23 degrees and, except for Fe, have a maximum at 10 degrees.

The angular distributions of the $^{13}C(^3He,^6He)^{10}C$ reaction to the $J^\pi = 0^+$ ground state and the $J^\pi = 2^+$ level at 3.35 MeV were measured by Kashy <u>et al</u>.[Ka73] in order to investigate the reaction mechanism in a case where both initial and final states are known. A zero-range distorted-wave Born-approximation calculation was performed which could not explain the shapes and relative magnitudes of the 0^+ and 2^+ transitions. Recently G. Delic and D. Kurath performed finite-range distorted-wave Born-approximation calculations[De76] which were more successful in describing the qualitative features of the reaction, particularly the ratio of the integrated cross-section of the 2^+ to that of the 0^+, $\sigma(2^+)/\sigma(0^+)$. In the finite-range DWBA calculation this ratio was calculated by Delic and Kurath to be of the order of 2-3 while the zero-range DWBA of Kashy <u>et al</u>. gave .4. Experimentally $\sigma(2^+)/\sigma(0^+)=4.5$ for the integrated cross sections up to $\theta_{cm}+45^\circ$. In order to achieve qualitative description of the shapes of the angular distributions, Delic and Kurath used different sets of optical model parameters for the 0^+ and 2^+ transitions. The description of the

(^{3}He,^{6}He) reaction by DWBA as a direct three neutron process is still a state of the art description which gives only qualitative results. In the current work, use was made of the angular distributions only as an empirical aid in determining the spin and parity of some levels. It is hoped that the data presented here will be useful as multi-nucleon transfer-reaction theory continues to improve.

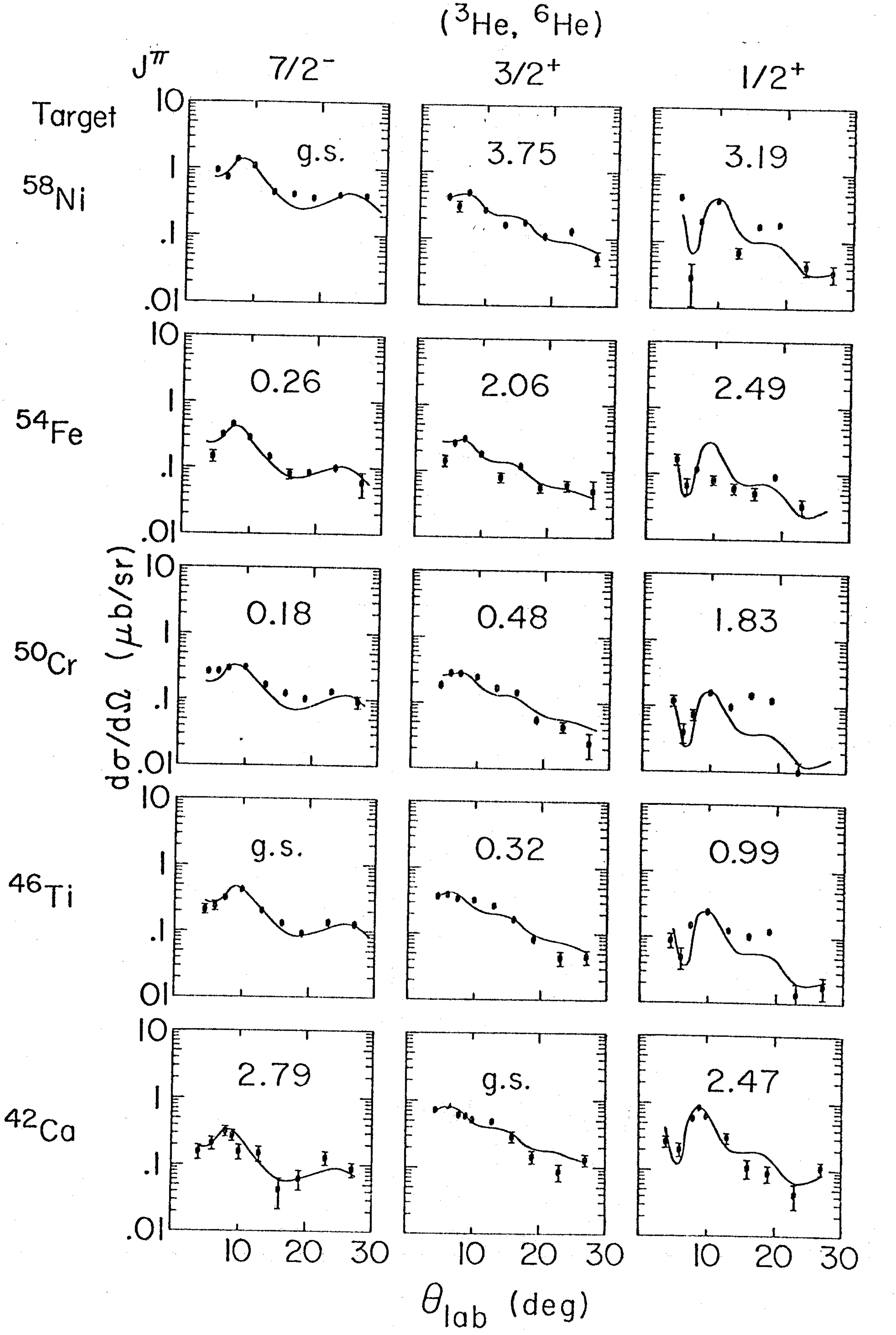

Figure 3.2.1 Angular distributions of the (^{3}He,^{6}He) reaction on ^{58}Ni, ^{54}Fe, ^{50}Cr, ^{46}Ti and ^{42}Ca. The curves represent an average of the ^{42}Ca and ^{58}Ni data. The ^{42}Ca data is from Nann *et al.*[Na76]

3.3 DISPLACEMENT ENERGIES

The measurement of the masses and excitation energies of these $T_z = \pm 1/2$ nuclei allows extraction of the displacement energies for the lowest $7/2^-$, $1/2^+$ and $3/2^+$ states of the $T = 1/2$ mirror pairs. The experimental displacement energy, ΔE_c, is:

$$\Delta E_c = M(T_z = +1/2) - M(T_z = +1/2) + .782 \text{ MeV}$$

$M(T_z = \pm 1/2)$ refers to the mass of the level in the $T_z = \pm 1/2$ nucleus and .782 MeV is the neutron-proton mass difference. Table 3.3.1 lists the experimental displacement energies of the $T = 1/2$ mirror pairs in the $1f_{7/2}$ shell having $J = 7/2^-$, $1/2^+$ and $3/2^+$ extracted from the current results those of Mueller _et_ _al_., and recent measurements of the corresponding $T_z = +1/2$ nuclei.[Jo74,No75, Jo76, No76] For a homogeneously charged sphere of radius R and charge Ze, the Coulomb energy is $E_c = 3/5[Z(Z-1)]e^2/R$. Thus, the Coulomb energy difference of two nuclei of charge $Z_<$ and $Z_<+1$, where $Z_<$ denotes the charge of the $T_z = +1/2$ nucleus, is $\Delta E_c = 6/5 \times e^2 Z_< /R$. By dividing ΔE_c by $Z_<$ the principal Z dependence of the displacement energy is removed, and the systematics can be examined in finer detail. Table 3.3.1 lists the experimental reduced displacement energies $E_c/Z_<$. Figure 3.3.1a shows a plot of $\Delta E_c/Z_<$ for the lowest $J^\pi = 7/2^-$ levels of the $T = 1/2$ mirror pairs in the $1f_{7/2}$ shell. The solid line indicates the results of a shell model calculation performed by W. Chung and B.H. Wildenthal[Ch75] who used the two-particle Coulomb interaction of Bertsch and Shlomo.[Sh74] The calculation assumed a pure $1f_{7/2}$ configuration and no change in the radial form factor for the nuclei from A = 41 to 55. There is a good agreement between the prediction and experiment for both the size of the Coulomb pairing interaction and the general dependence of the reduced Coulomb energy on A. The magnitude of the effective Coulomb pairing interaction for mass A is deduced from the masses of the nuclei by taking the difference between ΔE_c for A and the average of ΔE_c for A-1 and A+1. From the present data the average value of the Coulomb pairing interaction in the $1f_{7/2}$ shell is 62±10 keV. This small value would have been difficult to extract from less accurate mass measurements. Using the same procedure on the masses derived from the shell model calculation, a value of 44 keV is obtained for this pairing term, which is approximately 20 keV less than the empirical value. It is interesting to note that the 44 keV pairing deduced from the shell model results is significantly less than the 70 keV value entered in the two-body matrix elements of the shell model clode. This is due to seniority mixing since a good seniority scheme would have returned 70 keV as the Coulomb pairing interaction.

A plot of ΔE_c versus A for the lowest $5/2^+$ level in the $d_{5/2}$ shell is shown in Figure 2b. It is clearly seen that the $1f_{7/2}$ mirror states show considerably smaller Coulomb-pairing variations than is seen in the $1d_{5/2}$ shell. It has been pointed out by Sherr et al.[Sh65] that the size of the Coulomb energy difference varies more slowly than $A^{-1/3}$ in this region. The present data indicates an $A^{-1/n}$ dependence where $6 \leq n \leq 7$ throughout the $1f_{7/2}$ shell.

Table 3.3.1

Displacement energies and reduced displacement energies of the T=1/2 mirror pairs in the $1f_{7/2}$ shell.

A	J^{π}	ΔE_c(MeV)	$\Delta E_c/Z$	Refs.
41	$7/2^-$	7.278±0.005	0.3639±0.0002	Wa71
	$3/2^+$	7.364±0.009	0.3682±0.0005	Wa71,En73
	$1/2^+$	7.323±0.007	0.3662±0.0004	Wa71,En73
43	$7/2^-$	7.642±0.009	0.3639±0.0004	Wa71,present
	$3/2^+$	7.809±0.011	0.3718±0.0005	Wa71,En73,present
	$1/2^+$	7.947±0.013	0.3784±0.0006	Wa71,En73,present
45	$7/2^-$	7.906±0.018	0.3593±0.0008	Wa71,Mu75
47	$7/2^-$	8.262±0.010	0.3592±0.0004	Wa71,Sh74,present
	$3/2^+$	8.445±0.013	0.3672±0.0005	Wa71,Sh74,present
	$1/2^+$	8.397±0.013	0.3651±0.0005	Wa71,Sh74,present
49	$7/2^-$	8.487±0.018	0.3536±0.0008	Jo73,Mu75
51	$7/2^-$	8/846±0.011	0.3538±0.0004	Wa71,No76,present
	$3/2^+$	9.069±0.013	0.3628±0.0005	Wa71,No76,present
	$1/2^+$	9.036±0.013	0.3614±0.0005	Wa71,No76,present
53	$7/2^-$	9.073±0.023	0.3489±0.0009	Wa71,Mu75
55	$7/2^-$	9.477±0.010	0.3510±0.0004	Jo74,present
	$3/2^+$	9.703±0.012	0.3594±0.0004	Jo74,No75,present
	$1/2^+$	9.743±0.012	0.3609±0.0004	Jo74,No75,present

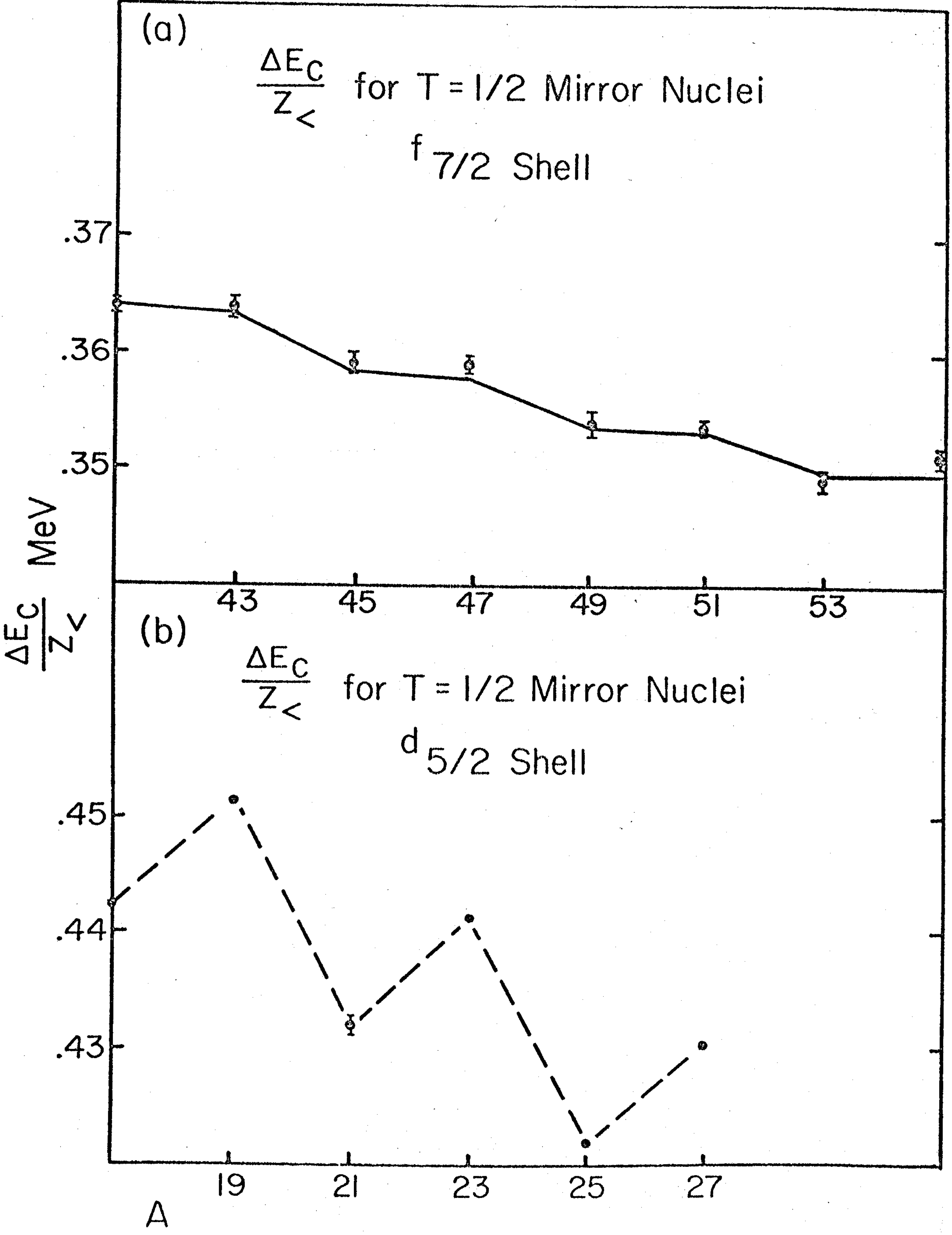

Figure 3.3.1 Graph of $\Delta E/Z_<$ versus A for T=1/2 mirror nuclei in the $f_{7/2}$ and $d_{3/2}$ shells. The points indicate the experimental data. The solid line indicates a shell model prediction of Chung and Wildenthal[Ch74] while the dashed line connects experimental points.

4.1 BFZ MODEL FOR DISPLACEMENT ENERGIES

Sherr and Bertsch have employed the Bansal-French-Zamick model (BFZ) to calculate the Coulomb displacement energies of excited particle-hole states in light nuclei and report that typically the level shifts are reproduced to within 50 keV.[Sh75] The BFZ model can be employed to find displacement energies by finding the difference between the binding energies of the particle-hole state and of its analogue. Under the assumption of charge symmetry and charge independence of the nucleon-nucleon interaction, the difference in the binding energy of the analogues is due to Coulomb effects. Under this assumption in the BFZ model, the binding energies of the nuclei can be replaced by their Coulomb energies, and only the Coulomb part of the particle-hole interaction need be considered.

For an m-particle-1-hole state the hole configuration is designated by H and the remaining core configuration by C. Then, the particle-hole state can be represented by $H \otimes C$, and the Coulomb energy of a state with isospin (T,T_z) is given by

$$E_c = \sum_i \left(T(C_i)\ T_z(C_i)\ T(H_i)\ T_z(H_i) \middle| T\ T_z\right)^2$$

$$\times \left(E_c(C_i) + E_c(H_i) - \upsilon_i \mu_i c\right)$$

The υ_i and μ_i are the numbers of proton holes and proton particles and c is the Coulomb interaction of a proton hole with a proton particle in a different shell. The index i is used to designate the constituent states necessary for a state of good isospin. In this model it is necessary to distinguish between A = 4n+1 and A = 4n+3 T = 1/2 mirror nuclei. For the latter case, the excited state H ⊗ C, is given by

$$\{(1h) \otimes (A+1)^{T=0}\} \quad T=1/2$$

For example in this model the nucleus ^{43}Ti in its $3/2^+$ excited state has the configuration:

$$(d_{3/2})^{-1} \begin{matrix} T=1/2 \\ T_z=1/2 \end{matrix} \otimes (f_{7/2})^4 \quad \begin{matrix} T=0 \\ T_z=0 \end{matrix}$$

The real nuclei which have the $d_{3/2}$ neutron hole in a ^{40}Ca core and 2-$f_{7/2}$ protons and 2-$f_{7/2}$ neutrons outside the ^{40}Ca core are ^{39}Ca and ^{44}Ti respectively. The mirror of ^{43}Ti is ^{43}Sc whose $3/2^+$ configuration is

$$(d_{3/2})^{-1} \begin{matrix} T=1/2 \\ T_z=-1/2 \end{matrix} \otimes (f_{7/2})^4 \quad \begin{matrix} T=0 \\ T_z=0 \end{matrix}$$

in this model. The real nuclei having these $(d_{3/2})^{-1}$ and $(f_{7/2})^4$ configurations about a ^{40}Ca core are ^{39}K and ^{44}Ti. Then, the Coulomb displacement energy of the lowest $3/2^+$ level in these A=43, T=1/2 mirror nuclei in this model is

$$\Delta E_c(43,3/2^+) = \Delta E_c(39,3/2^+) + 2c(3/2^+,7/2^-)$$

where $\Delta E_c(39,3/2^+)$ is the Coulomb energy difference of the

$3/2^+$ ground states of ^{39}Ca and ^{39}K, and $c(3/2^+,7/2^-)$ is the Coulomb interaction of a $d_{3/2}$ proton with an $1f_{7/2}$ proton. This method can be extended to the lowest $1/2^+$ states by employing $\Delta E_c(39,1/2^+)$ and $c(1/2^+,7/2^-)$. The results of calculations using this method for the A = 4n+3, T = 1/2 mirror nuclei with m-particle-1-hole states are given in Table 4.1.1 Three different methods of determining c were employed. First, the values of $c(3/2^+,7/2^-)$ =289keV. and $c(1/2^+,7/2^-)$ =286 keV determined by Sherr and Bertsch were used.[Sh75] Those values of c predict ΔE_c to be progressively smaller compared to the experimental values as the shell is filled. That is $\Delta = \Delta E_c\text{calc} - \Delta E_c$ exp. becomes smaller as A increases. Second, a least squares fit of c to the data was performed. The values obtained were $c(3/2^+,7/2^-)$ = 296 keV and $c(1/2^+,7/2^-)$ = 302 keV. These values improved the overall agreement with experiment, however the systematic trend in Δ still exists. Finally, the slope of ΔE_c versus A was fit. This leads to the even larger values of $c(3/2^+,7/2^-)$= 316 keV and $c(1/2^+,7/2^-)$ = 321 keV which remove the systematic trend of Δ. However, this is achieved at the cost of over-predicting ΔE_c by approximately 125 keV throughout the shell. This large difference may be due to the unusually large displacement energy of ^{39}K-^{39}Ca, which has been ascribed to the large binding energy of these nuclei.[Mu75b]

Figure 4.1.1 is a graph of ΔE_c vs A for the $3/2^+$ and $1/2^+$ levels in the $A = 4n+3$, $f_{7/2}$ shell nuclei. The solid line represents the calculated values of ΔE_c using $c(3/2^+,7/2^-),[c(1/2^+,7/2^-)] = 296$ keV [302 keV]. The dashed line represents the calculated ΔE_c with $c(3/2^+,7/2^-)$ $[c1/2^+7/2^-)] = 316$ keV [321 keV] with 126 keV [117 keV] subtracted from all the calculated $3/2^+$ $[1/2^+]$ levels. The dashed curves exhibit remarkable agreement with the data. The values 126 and 117 keV subtracted from the calculated values of ΔE_c agree with the increase of ΔE_c in mass 39 expected due to the large neutron separation of ^{39}K.[Mu75b] Finally, the $f_{7/2}$-$d_{3/2}$ and $f_{7/2}$-$2s_{1/2}$ Coulomb interaction was calculated using both harmonic oscillator and Woods-Saxon wave functions. Table 4.1.2 summarizes these calculations which exhibit approximate agreement with the experimentally derived Coulomb interactions.

Table 4.1.1 Displacement energies of m-particle-1-hole states of T=1/2, A=4n+3, $1f_{7/2}$ shell nuclei in keV.

A	J^{Π}	ΔE_c exp	ΔE_c calc$^{(1)}$	Δ	ΔE_c calc$^{(2)}$	Δ	ΔE_c calc$^{(3)}$	Δ
43	$3/2^+$	7.809(11)	7.882(5)	+73(12)	7.896(5)	+87(12)	7.936(5)	+127(12)
47	$3/2^+$	8.445(13)	8.460(5)	+15(14)	8.488(5)	+43(14)	8.568(5)	+123(14)
51	$3/2^+$	9.073(13)	9.038(5)	-35(14)	9.080(5)	-21(14)	9.200(5)	+127(14)
55	$3/2^+$	9.703(12)	9.616(5)	-87(13)	9.672(5)	-29(13)	9.832(5)	129(13)
43	$1/2^+$	7.785(13)	7.825(9)	+40(16)	7.857(9)	+72(16)	7.895(9)	+110(16)
47	$1/2^+$	8.397(13)	8.397(9)	+ 0(16)	8.461(9)	+64(16)	8.537(9)	+140(16)
51	$1/2^+$	9.040(13)	8.969(9)	-71(16)	9.065(9)	+33(16)	9.180(9)	+139(16)
55	$1/2^+$	9.743(12)	9.541(9)	-202(15)	9.669(9)	-72(15)	9.822(9)	+ 78(15)

(1) This set of calculations reflects the choice of Sherr and Bertsch of $C(3/2^+,7/2^-)=289$ keV. for the Coulomb interaction of a $d_{3/2}$ proton with a $f_{7/2}$ proton and $C(1/2^+,7/2^-)=286$ keV. for the $2s_{1/2}-f_{7/2}$ interaction.

(2) A least squares fit to the experimental displacement energies was performed to find $C(3/2^+,7/2^-)=296$ keV. and $C(1/2^+,7/2^-)=302$ keV.

(3) A least squares fit to the slope of the displacement energies was performed to find $C(3/2^+,7/2^-)=316$ keV. and $C(1/2^+,7/2^-)=321$ keV.

Table 4.1.2 Coulomb Interaction Between Shells

	Exp. (keV)	H.O.[a)] (keV)	W.S. (keV)	
			Direct	Exchange
$f_{7/2}-d_{3/2}$	316	308	338	-16
$f_{7/2}-2s_{1/2}$	321	294	328	- 6

a) Calculation made using the oscillator parameter $\nu = .258\ fm^{-2}$.

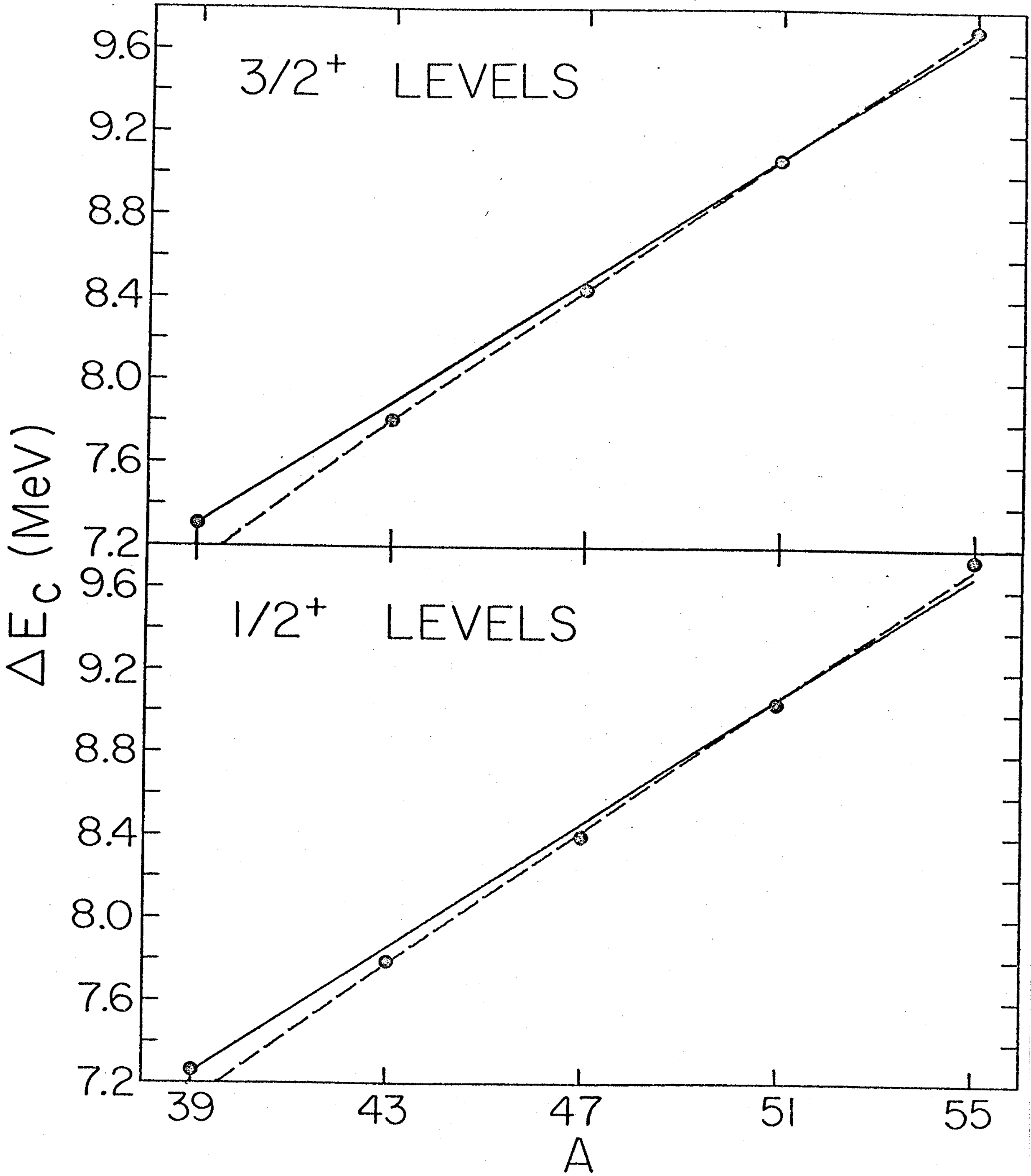

Figure 4.1.1 Plot of the Coulomb displacement energies of the lowest $3/2^+$ and $1/2^+$ levels of the A=4n+3, T=1/2 mirror pairs in the $f_{7/2}$ shell. The lines are the results of the calculations discussed in the text.

4.2 MASS PREDICTIONS

The current mass-excesses of the nuclei in the $f_{7/2}$ shell can be used to update the mass predictions based on the Garvey-Kelson symmetric mass relation[Ke66] of the proton-rich $f_{7/2}$ shell nuclei. This method, based upon an independent particle model, takes into account size, shell and pairing effects. In the cases where prediction and experiment can be compared, agreement at the 150 keV level is found with the largest deviations observed when nuclei from more than one sub shell are used in the relation. Table 4.2.1 lists the calculated mass excesses of 23 $T_z \leq -1$ isotopes from V through Ni which are predicted to be stable against alpha particle emission and against one or two-proton emission. Also listed are the first two isotopes predicted to be unbound to one or two-proton emission. In view of the predicted particle stability of ^{48}Ni and ^{45}Fe, it appears that the experimental observation of nuclei all the way out to the proton drip line will require some rather exotic heavy ion reactions and pose quite a challange to the experimentalists.

Table 4.2.1 Predicted mass excess using Garvey-Kelson symmetric mass relation.[a]

Nucleus	Mass excess (MeV)	Separation energy[b] (MeV) One proton	Two protons
		$T_z=-1$	
^{44}V	-23.83	1.81	6.31
^{46}Cr[c]	-29.56	5.02	6.64
^{48}Mn	-29.31	2.03	6.81
^{50}Fe	-34.50	4.13	6.22
^{52}Co	-34.38	1.48	6.34
^{54}Ni	-39.27	3.92	5.53
		$T_z=-\frac{3}{2}$	
^{43}V	-17.92	0.10	3.87
^{45}Cr	-19.64	3.14	4.95
^{47}Mn	-22.65	0.32	5.34
^{49}Fe	-24.76	2.76	4.79
^{51}Co	-27.40	0.19	4.32
^{53}Ni	-29.66	2.59	4.07
		$T_z=-2$	
^{42}V	- 8.02	-0.37	2.09
^{44}Cr	-13.54	2.96	3.06
^{46}Mn	-12.62	0.22	3.36
^{48}Fe	-18.17	2.82	3.14
^{50}Co	-17.73	0.26	3.02
^{52}Ni	-22.68	2.58	2.77
		$T_z=-\frac{5}{2}$	
^{41}V	0.08	-1.81	0.43
^{43}Cr	- 2.14	1.45	1.08
^{45}Mn	- 5.17	-1.14	1.82
^{47}Fe	- 7.15	1.84	2.06
^{49}Co	- 9.95	-0.93	1.89
^{51}Ni	-12.02	1.59	1.85
		$T_z=-3$	
^{42}Cr	6.17	1.25	-0.56
^{44}Mn	6.35	-1.26	0.19
^{46}Fe	0.53	1.60	0.46
^{48}Co	0.97	-0.84	1.00
^{50}Ni	- 4.13	1.49	0.56

$T_z=-\frac{7}{2}$			
^{45}Fe	13.58	0.08	-1.18
^{49}Ni	7.61	0.67	-0.17
$T_z=-4$			
^{48}Ni	16.43	0.50	-1.31

---

a) Masses used in the relation are the present experimental results, Mass 71 mass values of A.H. Wapstra and N.B. Gove, Nucl. Data A9, 267(1971), for the ^{55}Co mass excess is -54.0275±0.0022 MeV from P.L. Jolivette et al. Phys. Rev. C10, 2449(1974) and for the mass excess of ^{49}Cr is -45.327±0.0029 MeV from P.L. Jolivette et al. private communication and Phys. Rev. C13, 439 (1976).

b) Negative binding energy indicates nucleus unbound to particle emission.

c) Experimental mass excess is -29.46±0.03 J. Zioni et al. Nucl. Phys. A181, 465(1972).

APPENDIX A

DETECTOR DEVELOPMENT

Previously resistive-wire-proportional counters have been used successfully at the Michigan State University Cyclotron Laboratory and elsewhere.[Fu73] However, position resolution has been limited for particles incident at 45° to the counter to full widths at half maxima of 1.8 mm. for 35. MeV protons, 0.8 mm. for 25 MeV deuterons and 0.6 mm. for 25 MeV alphas. There are three difficulties to be overcome in improving these counters. The first is the lack of isolation between the preamps at each end of the coil, which limits the signal-to-noise ratio. Second is straggling which causes an uncertainty in the position of particles with non-normal incidence. Straggling affects the position since a particle with non-normal incidence that loses more energy on one side of the wire than on the other would have its position signal shifted. Third is small angle scattering by the entrance window of the counter and by the gas in the counter. The effect on observed resolution caused by both straggling and by small angle scattering is calculable and can be reduced by employing a thinner detector; however, the signal-to-noise ratio is made worse by using a thinner detector. The effect due to straggling can be reduced by using higher gas pressure in the detector, but this increases the small angle scattering in the gas and necessitates using a higher voltage on the central wire. Finally, the size of all three effects is dependent on both the particle type and its energy. The design and performance of two variations of the resistive-wire-proportional counter will be discussed.

The first detector to be discussed was designed to give best results for 50 MeV. ^{6}He particles. This detector has an active region that is 1.0 cm. thick by 1.4 cm. high by 18 cm. long. The entrance window is .013 mm. thick aluminized Kapton which defines the front surface of the active region of the counter. The exit window is 250 $\mu g/cm^2$ Al leaf which defines the back surface of the counter and separates it from a second proportional counter. The central wire is .0076 mm. diameter nichrome wire that has a resistance of 3400 ohms (19 ohm/mm). This wire is thinner than the .0124 mm. diameter wire previously used, and has approximately 1.6 times the resistance per unit length of that previously used, thereby improving the signal-to-noise ratio. Also, the wire is of better quality, and it gives uniform charge multiplication along its entire length. The block diagram of the electronics for this detector, shown in Figure 2.1.1 also illustrates the electronics for the particle identification system used in conjunction with this detector.

The contribution to the FWHM of the observed peak from straggling is proportional to the square root of the counter thickness and inversely proportional to the square root of the pressure of the gas used in the counter. A calculation of the contribution from straggling for this counter and a pressure of .67 atm. of propane gives .25 mm. for 50 MeV ^{6}He particles at 45° incidence.[Ma75] The contribution to the resolution from small angle scattering is calculated[Ja62, Ma75, Mi74] to be less than .1 mm. for scattering from the Kapton window and less than .03 mm. for the propane. In the gas, the rms. deviation in position due to scattering in the first 5 mm. of gas was calculated. Scattering in the second 5mm. of gas was neglected. For 77 MeV alpha particles, and therefore, for the more ionizing ^{50}MeV ^{6}He particles, the signal-to-noise ratio is not a limiting factor in this detector. This was checked experimentally by measuring the resolution as a function of amplifier gain.

The amplifier gain was varied by a factor of 5 while adjusting the gas gain by changing the high voltage and no change in resolution was observed. The resolution deteriorated at gains above and below these limits. Figure 3.1.7 shows a spectrum of ^{6}He particles in which 30 keV resolution was obtained. This corresponds to .6 mm. full width at half maximum. The energy loss in the 82 $\mu g/cm^2$ ^{50}Cr target contributes only 6 keV. (~.1 mm.) to the peak width while small angle scattering in the target contributes only 2 keV to the width. The sum of the contributions to the resolution from the target and from the detector is only half that obtained experimentally. This indicates a significant contribution to the peak width from the incident beam and that a better dispersion matching situation could improve the resolution substantially.

The second detector is a novel design which employs a thin coil of 7000 ohms resistance, which defines the active region of the counter, and a central wire. The coil has a rectangular cross-section, dimensions of 1.27 cm. high by 0.4 cm. wide by 6.2 cm. long and turn spacing of 1.3 mm. Nichrome wire of .178 mm. diameter was used for both the coil and central wire. Photographs of the detector are shown in Figure A.1, and Figure A.2

shows a block diagram of the electronics. Windows of aluminized Kapton were used. The detector is filled with a gas mixture of 5% CO_2, 9.5% He and 85.5% Ne at two atmospheres absolute pressure. A bias of +900 volts is used on the central wire and -400 volts on the coil. In operation the center wire acts as a proportional counter producing charge multiplication, and the coil picks up the complimentary positive signal. The position is then determined by division of the signal from one end of the coil by the sum of the signals from both ends of the coil. The results of testing this counter indicate that the observed peak width varies with position periodically as the turn spacing. The bottom half of Figure A.3 shows a proton peak that is 3 times as broad as that in the upper half. The only difference in the experimental setup between the two was that the spectrograph field was changed in order to move the peak position .6 mm. (one half the turn spacing!). Moving the peak an additional .6 mm. causes the peak to become broad again. This experimental evidence suggests that the use of such a coil-type counter is of questionable value if the turn spacing is the same size or larger than the peak width being observed.

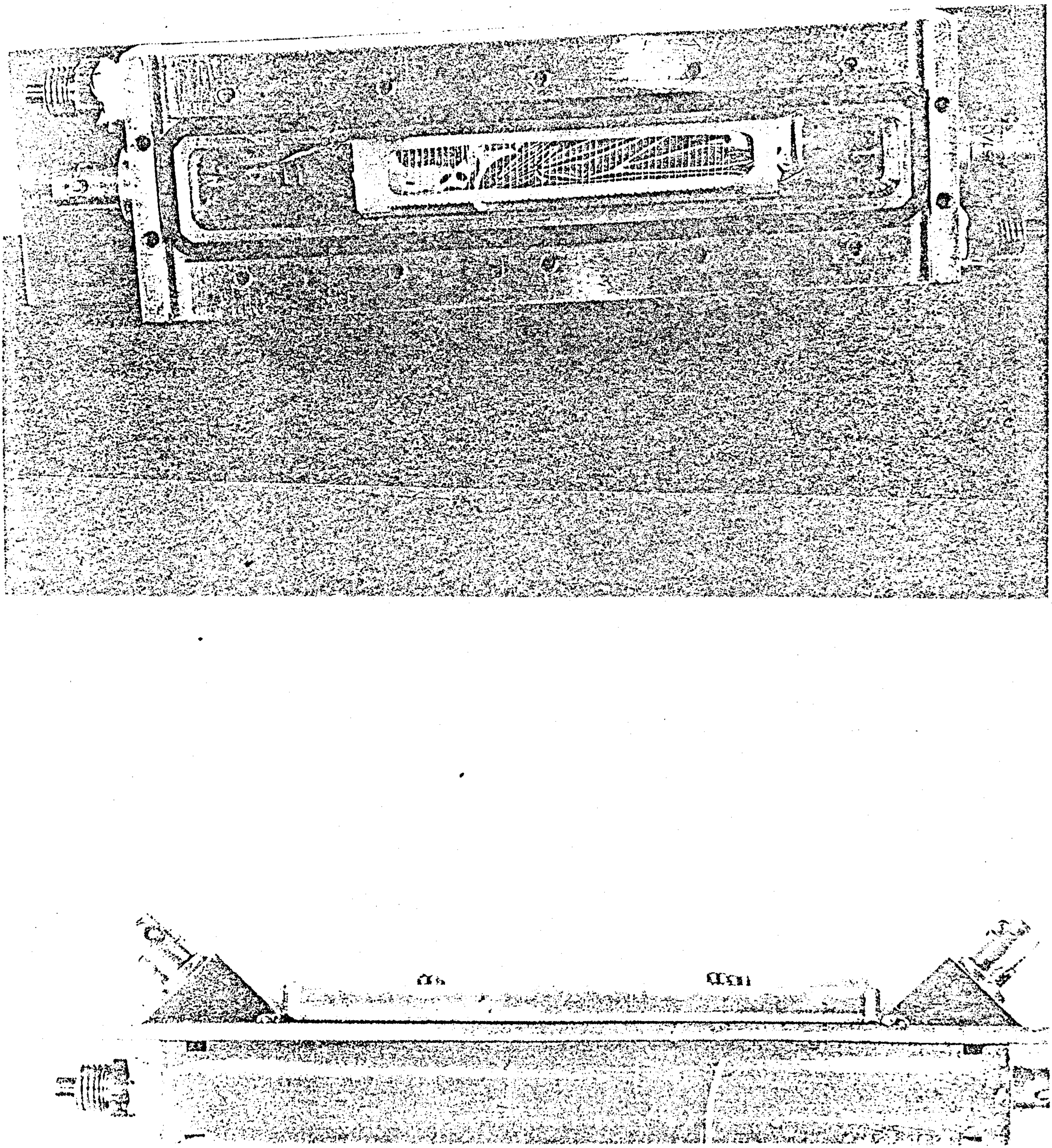

Figure A.1 Photograph of coil detector.

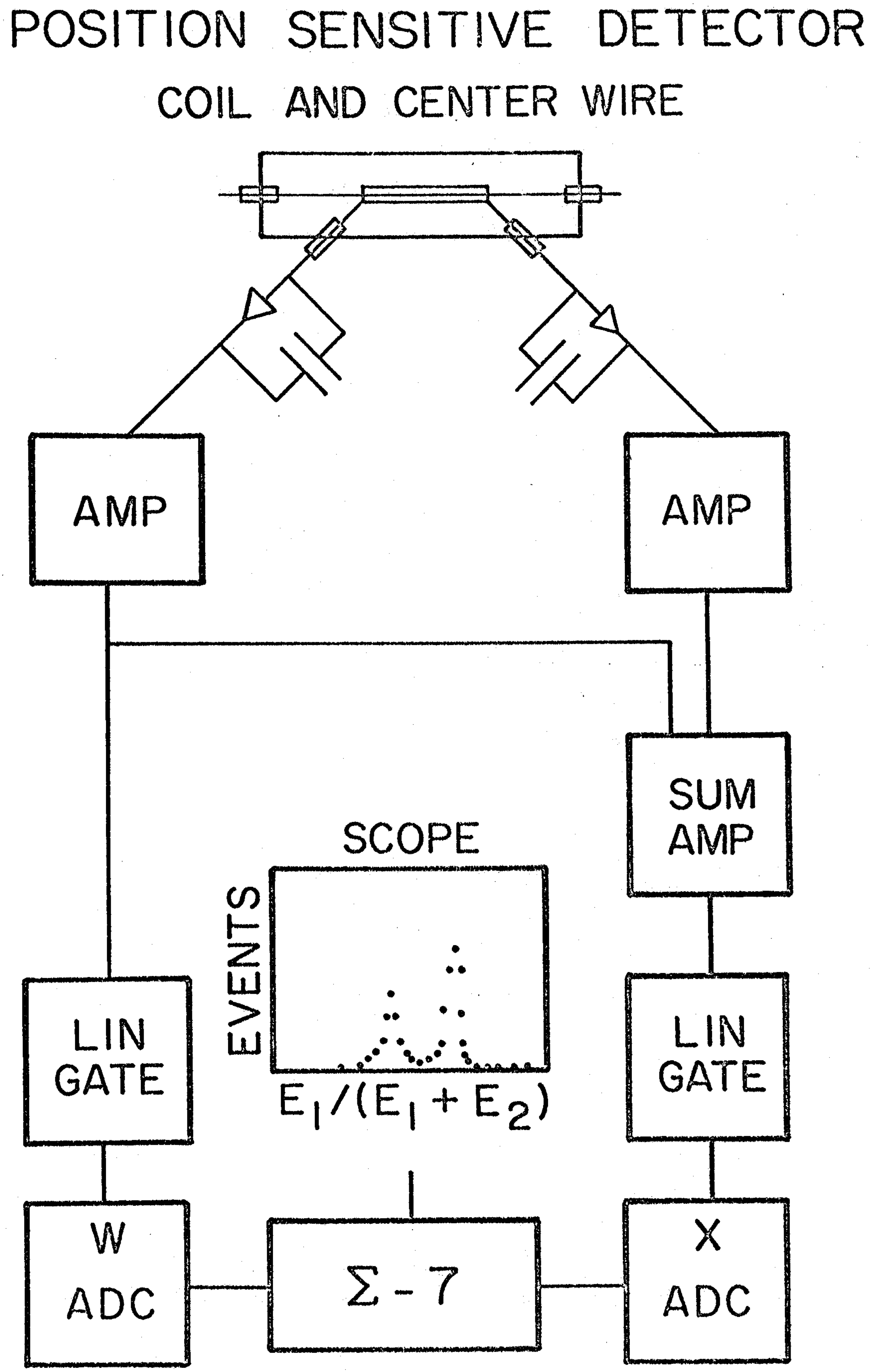

Figure A.2 Block diagram of the electronics of the coil detector.

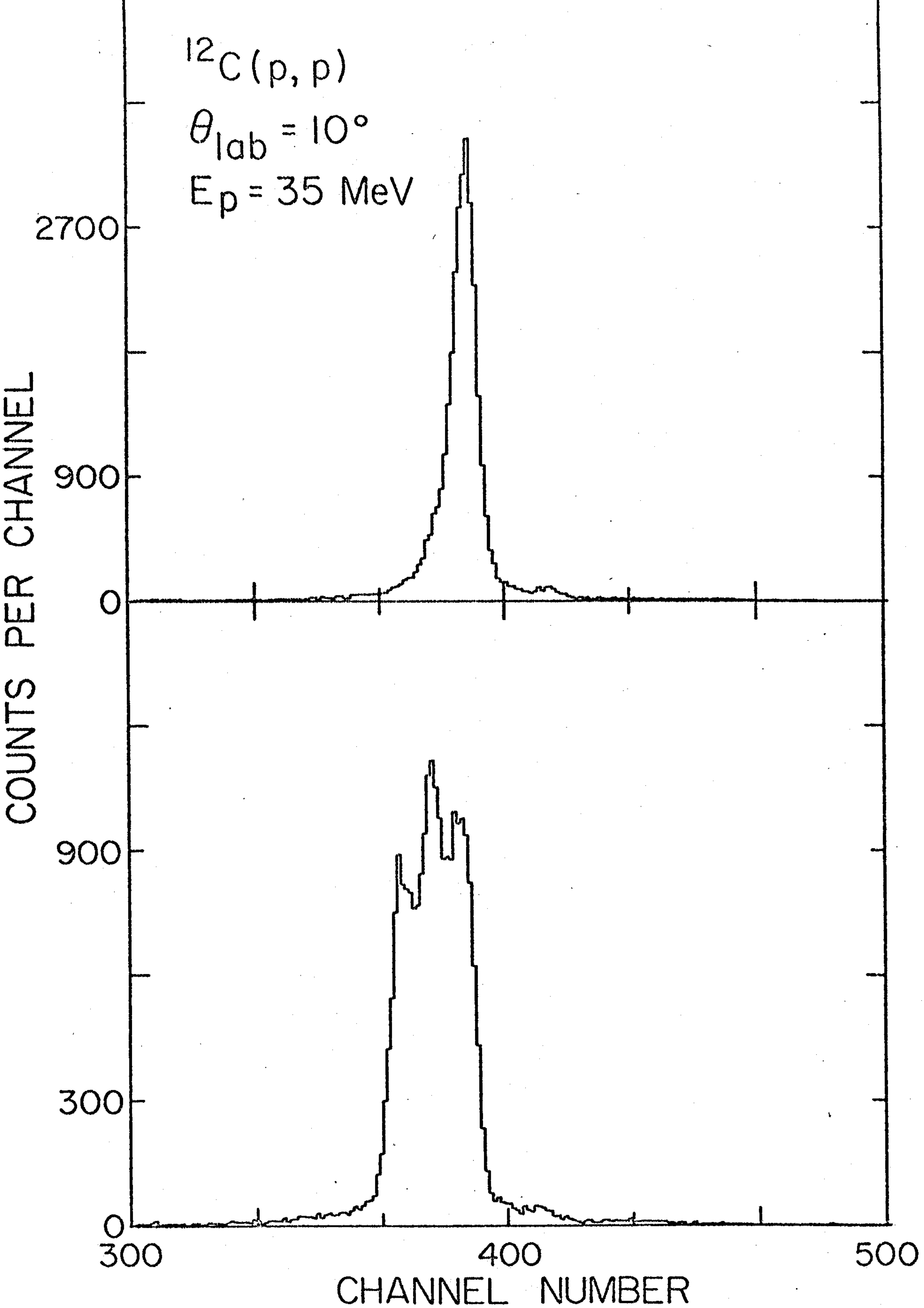

Figure A.3 Peak of 35 MeV protons elastically scattered from ^{12}C which was detected with the coil counter described in the text. The difference between the two peaks is that their positions differ by one-half the turn spacing of the coil.

APPENDIX B

MASS OF ^{57}Ni

In order to check an inconsistency found during the analysis of the (^{3}He,^{6}He) data, the ^{58}Ni(^{3}He,^{4}He)^{57}Ni Q-value was measured. The experimental technique used was that which is described in the main body of this thesis. The magnetic rigidities of the alpha particles from the ^{58}Ni(^{3}He,^{4}He)^{55}Ni reaction were compared to those from the ^{52}Cr(^{3}He,^{4}He)^{51}Cr reaction. The targets employed were isotopically-enriched evaporated targets on Carbon backings. The target thicknesses were measured by means of the energy-loss of ^{241}Am alpha particles. Several runs were made on both the ^{58}Ni and ^{52}Cr targets. Table B.1 lists the target thickness, the Q-value of the reactions and the mass excess of ^{57}Ni determined from the average of all the runs. The result for the ^{57}Ni mass excess is 24 keV more positive than the Mass-71 value[Wa71], and the error has been reduced from 7 to 4.6 keV.

Table B.1

Reaction	Target Thickness ($\mu g/cm^2$)	Q-Value (MeV)	Mass Excess of Residual Nucleus (MeV)
$^{52}Cr(^3He,^4He)^{51}Cr$	50(10)	+8.5378(22)[a]	-51.4460(10)[a]
$^{58}Ni(^3He,^4He)^{57}Ni$	90(10)	+8.3603(40)	-56.0804(46)[b],[c]

a) Mass excesses of -55.4149(19) and -51.4460(10) MeV for ^{51}Cr from Ref. Jo74 were used.

b) The mass excess of -60.2268(21) MeV for ^{58}Ni from Ref. Jo74 was used.

c) The previous value for the ^{57}Ni mass excess was -56.104(7).[Wa71]

LIST OF REFERENCES

Aj75 F. Ajzenberg-Selove, Nucl. Phys. A248, 1 (1975).

Al67 A. M. Aldridge, H. S. Plendl and J. P. Aldridge, III, Nucl. Phys. A98, 323 (1967).

Au72 N. Auerbach, J. Hufner, A. K. Kerman and C. M. Shakin, Rev. Mod. Phy. 44, 48 (1972).

Au76 Computer codes written by R. Au and D. Mueller, Michigan State University.

Bo69 A. Bohr and B. R. Mottelson, Nuclear Structure, Vol. I (W.A. Benjamin, Inc., New York, 1969) pp. 138 & 142.

CH74 W. Chung and B. H. Wildenthal, Private communication.

Co67 H. R. Collard, L. R. B. Elton and R. Hofstadter, Nuclear Physics and Technology; nuclear radii, ed. H. Schopper (Springer-Verlag, 1967) p. 34.

Co53 L. N. Cooper and E. M. Henley, Phys. Rev. 95, 717 (1953)

De76 G. Delic and D. Kurath, Preprint LBL-5364, Submitted to Phys. Rev. C.

En73 P. M. Endt and C. van der Leun, Nucl. Phys. A214, 1 (1963)

Ev55 R. D. Evans, The Atomic Nucleus (McGraw-Hill Book Company, 1955) ch. 2.

Fu73 H. Fulbright, R. G. Markham and W. A. Lanford, Nucl. Instrum. Meth. 108, 125 (1973).

Ha74 J. C. Hardy, H. Schmeing, W. Benenson, G. M. Crawley, E. Kashy, and H. Nann, Phys. Rev. C9, 252 (1974).

Ja62 J. D. Jackson, Classical Electrodynamics, (John Wiley and Sons, Inc., New York, 1962) pp. 456-459.

Ja69 J. Jänecke, Isospin in Nuclear Physics, ed. D. H. Wilkinson (North-Holland, Amsterdam, 1969) ch. 8.

Jo74 P. L. Jolivette, J. D. Goss, G. L. Marolt, A.A. Rollefson and C. P. Browne, Phys. Rev. C10, 2449 (1974).

Jo76 P. L. Jolivette, J. D. Goss, J. A. Bieszk, R. D. Hichwa and C. P. Browne, Phys. Rev. C13, 439 (1976).

Ka73 E. Kashy, W. Benenson, I. D. Proctor, P. Hauge and G. Bertsch, Phys. Rev. C7, 225 (1973).

Ke66 I. Kelson and G. T. Garvey, Phys. Lett. 23, 689 (1966).

Ko68 Computer code written by J. Kolata, Michigan State University (1968) and M. J. Berger and S. M. Seltzer, NAS-NRC Publication 1133; USAEC NAS-NS 39, 188 (1964).

Lo76 W. G. Love and S. Shlomo, Preprint Michigan State University.

Ma75 R/ G. Markham and R. G. H. Robertson, Nucl. Instrum. Meth. 129, 131 (1975) and private communication.

Mi74 Computer code written by P. S. Miller, Michigan State University.

Mi76 P. S. Miller and D. Johnson, private communication.

Mu75 D. Mueller, E. Kashy, W. Benenson and H. Nann, Phys. Rev. C12, 51 (1975).

Mu75b D. Mueller, E. Kashy and H. Nann, Phys. Lett. 59B, 223 (1975).

Na76 H/ Nann, E. Kashy and D. Mueller, to be published.

ND73 Nuclear Data Group, Nuclear Level Schemes A= 45 through A=257 (Academic Press, 1973).

Ne71 J. W. Negele, Nucl. Phys. A165, 305 (1971).

Ne74 J. W. Negele, Invited talk International Conference on Nuclear Structure and Spectroscpy, Amsterdam, 1974 (MIT Publication #431), Comments on Nucl. and Part. Phy. VII, ;5 (1974).

No69 J. A. Nolen, Jr. and J. P. Schiffer, Ann. Rev. Nucl. Sci. 19, 471 (1969).

No70 L. C. Northcliffe and R. F. Schilling, Nucl. Data A7, 223 (1970).

No74 J. A. Nolen, Jr., G. Hamilton, E. Kashy and I. D. Proctor, Nucl. Instrum. Meth. 115, 189 (1974).

No75 J. A. Nolen, Jr., J. Finck, P. Smith and R. Sherr, Private communication.

No76 J. W. Noē, R. W. Zurmühle and D. P. Balamuth, Private communication.

Ok71 K. Okamato and C. Pask, Ann. of Phy. 68, 18 (1971).

Ov69 J. C. Overly, P. D. Parker and D. A. Bromley, Nucl. Instrum. Meth. 68, 61 (1969).

Sa73 H. Sato, Preprint University of Michigan Physics Dept.

Sh65 R. Sherr, B. F. Bayman, E. Rost, M. E. Rickey and C. E. Hoot, Phys. Rev. B139, 1273 (1965).

Sh72 S. Shlomo, Phys. Lett. 42B, 146 (1972).

Sh73 S. Shlomo, Ph.D. thesis, Weizman Institute (1973).

Sh74 S. Shlomo and G. Bertsch, Phys. Lett. 49B, 401 (1974) and Private communication.

Sh74b N. Schultz and M. Toulemonde, Nucl. Phys. A230, 401 (1974).

Sh75 R. Sherr and G. Bertsch, Phys. Rev. C12, 1671 (1975).

Sh75b S. Shlomo and D. O. Riska, Nucl. Phys. A254,281 (1975).

Sh76 D. L. Show, B. H. Wildenthal, J. A. Nolen, Jr. and E. Kashy, accepted by Nucl. Phys.

Sn67 J. L. Snelgrove and E. Kashy, Nucl. Instrum. Meth. 52, 153 (1967(.

Tr70 G. F. Trentelman and E. Kashy, Nucl. Instrum. Meth. 82, 304 (1970).

Wa71 A. H. Wapstra and N. B. Gove, Nucl. Data A9, 267 (1971).

We35 C. F. von Weizsäcker, Z. Physics 96, 431 (1935).

Wi66 C. F. Williamson, J. Boujot and J. Picard, Centre D'Etudes Nucleaires De Saclay, Rapport C.E.A.-R3042 (1966).